

Sensors and Actuators B: Chemical
Hybrid cement composite-based sensor for in-situ chloride monitoring in concrete structures
--Manuscript Draft--

Manuscript Number:	SNB-D-22-06910R1
Article Type:	Research Paper
Section/Category:	Electrochemical Sensors
Keywords:	Geopolymer cement; Graphene; chloride sensor; electrochemical spectroscopy.
Corresponding Author:	Bo Huang CHINA
First Author:	Bo Huang, PhD
Order of Authors:	Bo Huang, PhD Jianqun Wang, PhD Gabor Piukovics Niloufar Zabihi, PhD Junjie Ye, PhD Mohamed Saafi, PhD Jianqiao Ye, PhD
Abstract:	In this paper, we present a rugged cementitious composite sensor for monitoring chloride ingress in concrete structures. The sensor is in the form of an electrochemical double-layer, consisting of a chloride ion-selective functionalized graphene film sandwiched between two cementitious composites. The cementitious composite chloride sensor was subjected to different chlorides concentrations and electrochemical impedance spectroscopy (EIS) measurements were conducted to characterize its response. The effect of the pore solution and the independent impact of temperature and humidity on the sensor's response were also quantified. The experimental results showed that the sensor successfully measured chlorides concentration changes with good sensitivity. The sensor's response was not affected by temperature and humidity and showed good reversibility and stability. However, the pH of the pore solution affected the sensor's response to chlorides and a sensor calibration equation that considers pH is proposed. The characterization work presented herein provides a base for the development of such chloride sensing method, which can provide useful information for chloride diffusion models updating and health monitoring of the concrete structures subjected to sodium chloride.
Response to Reviewers:	

Responses to reviewers' comments

Journal: Sensors and Actuators B: Chemical

Manuscript number: SNB-D-22-06910

Title: Hybrid cement composite-based sensor for in-situ chloride monitoring in concrete structures

Authors: Bo Huang, Jianqun Wang, Gabor Piukovics, Niloufar Zabihi, Junjie Ye, Mohamed Saafi, Jianqiao Ye

The authors would like to express their gratitude to the reviewers for their time and efforts in reviewing our manuscript. Their remarks and valuable suggestions have been instrumental in improving the quality of the paper. All the comments have been addressed in the revised manuscript. A detailed list of the point-by-point responses to the comments is given below. The basic format follows the sequence: Comments, Reply and Corrections. The [revised text is highlighted in blue](#) for easy identification.

Responses to Reviewer #1

No.	Comments, Reply and Corrections	
1.	Comments	<i>The authors propose an innovative graphene chloride sensors based on EIS. The introduction defines clearly the context of the study with respect to the state or arts: separating the chloride content / temperature / humidity / alkalinity parameters. The large amount of results are well described and explained. As shown, humidity and temperature do not affect the results. Although it is not possible to separate fully chloride and alkalinity sensitivities, a discussion on the interference of these two parameters is made. Due to these interesting results, I recommend to accept the paper in its current form.</i>
	Reply	I would like to thank the reviewer for the comments. . .
	Corrections	No specific changes were made based on these comments.

Responses to Reviewer #2

No	Comments, Reply and Corrections	
1.	Comments	<i>This is potentially publishable paper. However, its actual form is technically poor.</i> <i>Question:</i> <i>Especially the sensor construction and its experimental setup shown in Figures 1, 2 and 3 are confusing.</i>
	Reply	We thank the reviewer for the comments. The figures 1, 2 and 3 were modified and clarified as requested (pages 13-14).

Corrections

We have made corrections to Figure 1-3.

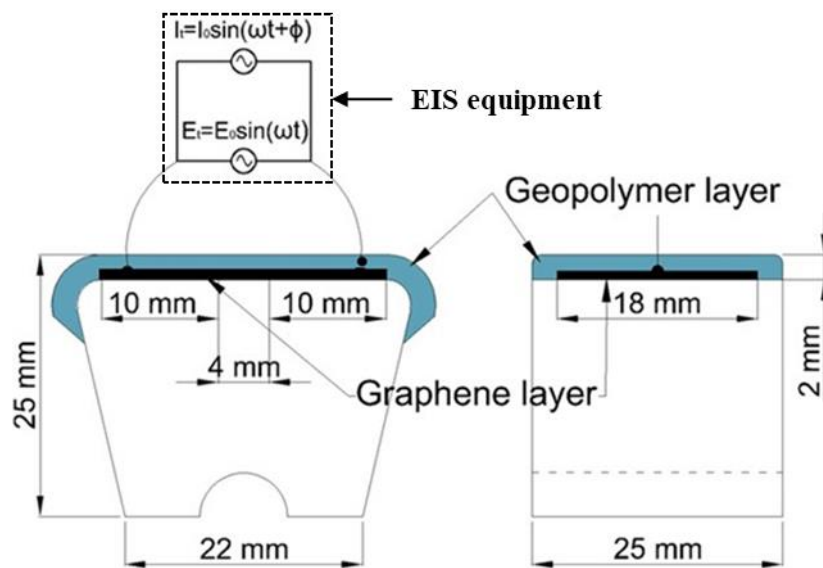


Fig. 1. Layout and size of the chloride sensor.

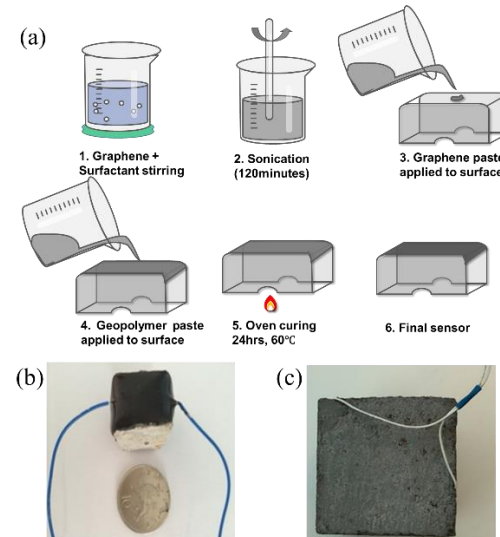


Fig. 2. Chloride sensor (a) manufacturing process, (b) completed chloride sensor, (c) concrete cube with the embedded sensor.

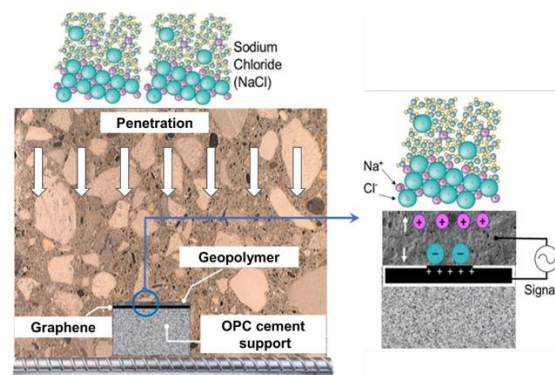


Fig. 3. Chloride sensor working principle.

		,
2.	Comments	<p>The text in several places is puzzling; for illustration just three examples are given here:</p> <p>a) Introduction: "Chlorides (Cl^-) penetration in concrete is typically the result of the water diffusion containing sodium chloride (NaCl) in concrete".</p> <p>b) Section 2.2: "NaCl ions"</p> <p>c) Section 2.4: "30% potassium hydroxide with pH levels of 12, 13 and 14"</p>
	Reply	The authors improved the readability of the text.
	Corrections	<p>The corrections have been made in the text; and the following text is corrected in the Introduction (page 2), Section 2.2 (page 4) and Section 2.4.</p> <p>'Chlorides (Cl^-) penetration into concrete typically occurs when water containing sodium chloride (NaCl) diffuses into the concrete.'</p> <p>The Na^+ and Cl^- ions diffuse through the porous protective geopolymers layer and interact with the functionalized graphene film.</p> <p>The concrete cube with the embedded sensor was placed in a glass container filled with a solution consisting of mixture of 70% NaCl solution and 30% sodium hydroxide solution. The concentrations of Cl^- were 10, 20, 40, 60 and 100 mM/L, and the pH levels of the sodium hydroxide solution with pH levels of 12, 13 and 14.'</p>
3.	Comments	<p>Figure legends are incomplete and rather messy, and the ms. text in several places is not clear enough. Also, the impedance parameters should be clearly named in the figures.</p>
	Reply	We thank the reviewer comments and suggestions. To avoid confusion, we have updated the figure legends, manuscript and impedance parameters in Fig.4 (page 14), Fig.6 (page 15), Fig.7 (page 16), Fig.9 (page 17), Fig.11 (page 18), Fig.15 and Fig.16 (page 20), respectively.
	Corrections	<p>We have made corrections to the manuscript text and updated the following figures: Fig. 4, Fig.6, Fig.7, Fig.9, Fig.11, Fig.15 and Fig.16.</p> <p>(a)</p> <p>(b)</p> <p>Fig. 4. Experimental test set up for the sensor subjected to NaCl solution.</p>

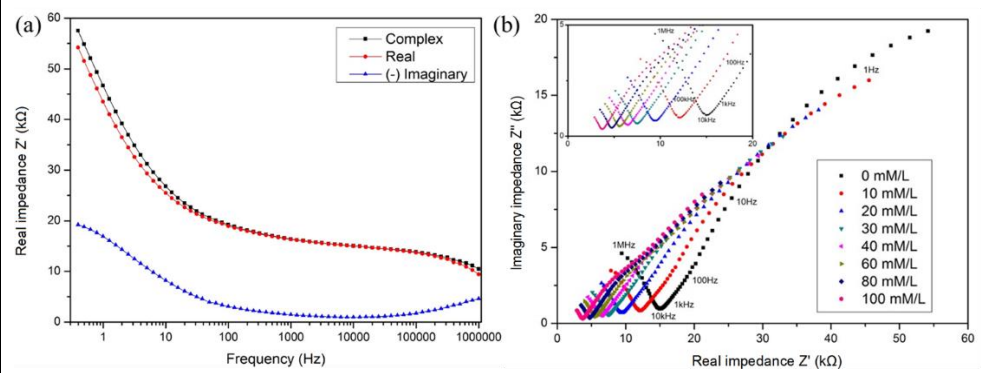


Fig. 5 Impedance of the sensor at room temperature (a) Bode plot prior exposure to chloride, (b) Nyquist plot at different Cl^- concentrations.

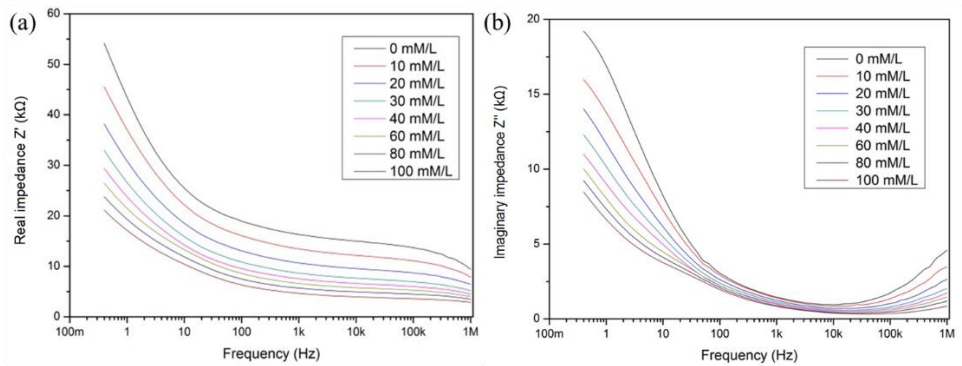


Fig. 6. Bode plot of the sensor at different Cl^- concentrations (a) real impedance, (b) imaginary impedance.

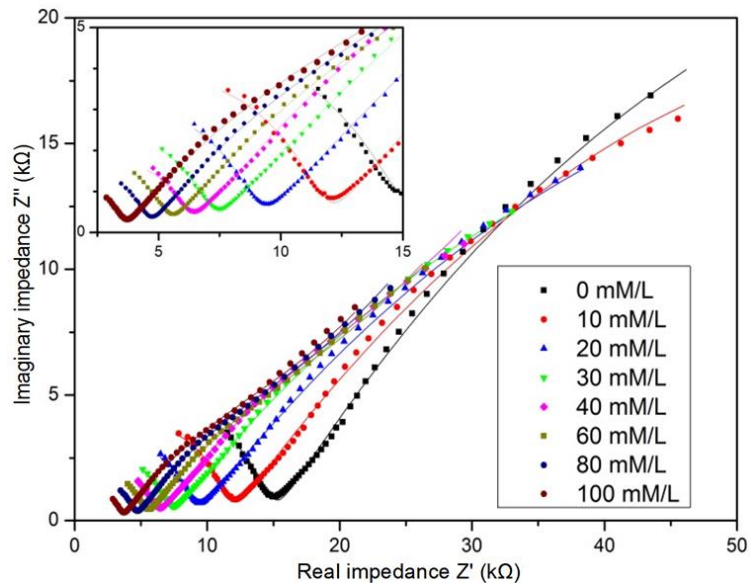


Fig. 7. Nyquist plots for the sensor at different Cl^- concentrations and the corresponding equivalent circuit (solid lines).

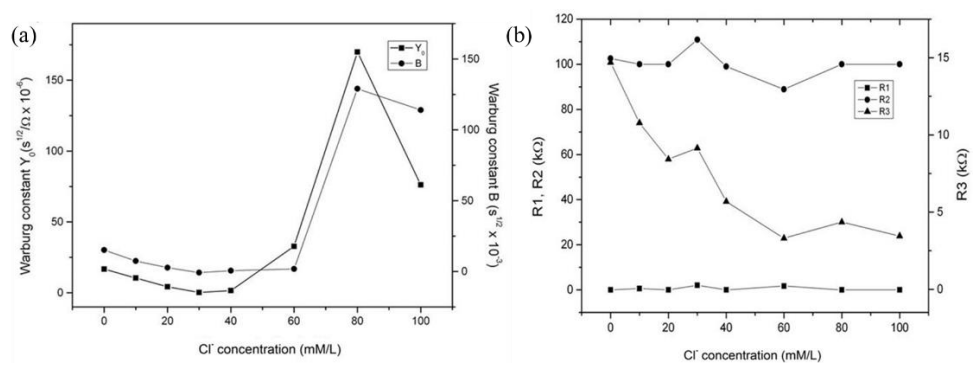


Fig. 8. Effect of Cl^- concentrations on the equivalent circuit parameters for the sensor (a) Warburg elements Y_0 and B , and (b) R_1 , R_2 and R_3 .

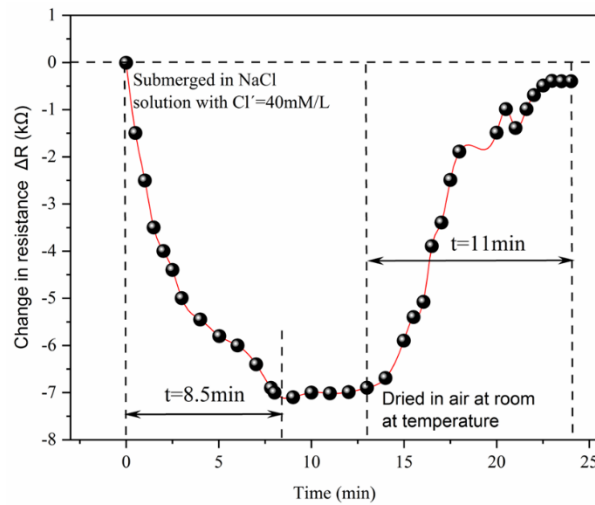


Fig. 9 Reversibility of the sensor under one wet-dry cycle at 1 kHz and 40 mM.

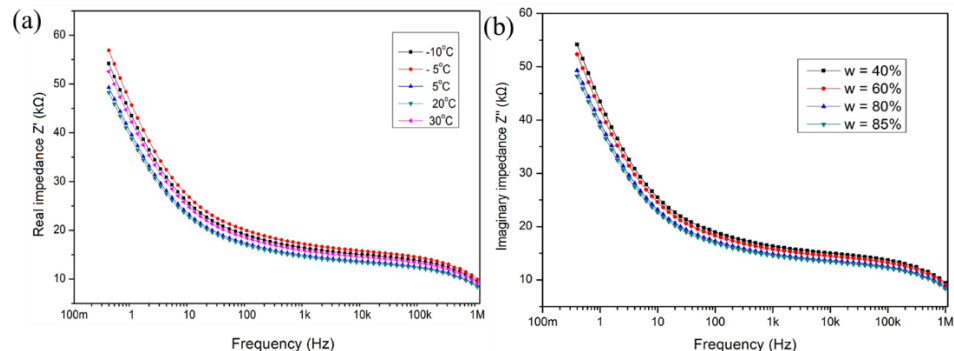


Fig. 10 Sensor at 1 kHz response effect of (a) temperature, (b) humidity.'

4.	Comments	<i>Figure 13: the correlation coefficients are rather poor.</i>
	Reply	Thank you for your comments. We used linear regression to obtain the simplest relationship between the variables. After careful consideration, we adopted non-linear curve lines to fit the data, as shown in Fig.13. The new correlation coefficients are 0.99. Corrections to the text (lines 2, 5 and 8, on page 10), and fig.13 on page 19.

	Corrections	<p>Corrections have been made in the text and the following fig. 13. ‘The non-linear curve lines of best fit and their equations are illustrated in Fig. 11.</p> <p>A general equation of the fitted lines can be expressed as:</p> $Z' = -Z_0 Cl^- + Z_1(Cl^-)^2 + Z_2 \quad (5)$ <p>From Fig. 11, it can be observed that Z_0 (approximately 0.2 kΩ/mM) and Z_1 (approximately 0.01 kΩ/mM) remain constant over the entire pH range, whereas Z_2 is highly dependent on the pH level and decreases as the pH increases.</p>
5.	Comments	<p><i>One of the final conclusions "The sensors could be deployed in the form of a wireless(?) sensor network" is not sufficiently supported.</i></p>
	Reply	<p>We thank the reviewer for their comment. After careful consideration, we have decided to removed “<i>The sensors could be deployed in the form of a wireless sensor network</i>” and make the necessary corrections to the conclusions.</p>
	Corrections	<p>The necessary corrections have been made in the conclusion (Lines 14-17, Page 12).</p> <p>‘The sensors could be deployed in the form of a structural health monitoring system to continuously measure chloride contents in concrete. The information can be used to update the parameters of chloride diffusion models for the prediction of corrosion initiation, maintenance, and service-life performance of concrete structures.’</p>

- Novel chloride sensor synthesised from hybrid cementitious composites.
- The sensor exhibited high sensitivity to chloride.
- The sensor showed good stability and repeatability.
- The sensor response was not affected by temperature/humidity but was sensitive to pH.
- Calibration equation that considers OH^- interference is proposed.

Hybrid cement composite-based sensor for in-situ chloride monitoring in concrete structures

Bo Huang^{a,b*}, Jianqun Wang^{a*}, Gabor Piukovics^b, Niloufar Zabihi^b, Junjie Ye^c, Mohamed Saafi^{b*}, Jianqiao Ye^b

^aSchool of Civil Engineering, Hunan University of Science and Technology, Xiangtan, 411201, China

^bDepartment of Engineering, Lancaster University, Lancaster, LA1 4YR, UK

^cResearch Center for Applied Mechanics, Key Laboratory of Ministry of Education for Electronic Equipment Structure Design, Xidian University, Xi'an 710071, China

Abstract

In this paper, we present a rugged cementitious composite sensor for monitoring chloride ingress in concrete structures. The sensor is in the form of an electrochemical double-layer, consisting of a chloride ion-selective functionalized graphene film sandwiched between two cementitious composites. The cementitious composite chloride sensor was subjected to different chlorides concentrations and electrochemical impedance spectroscopy (EIS) measurements were conducted to characterize its response. The effect of the pore solution and the independent impact of temperature and humidity on the sensor's response were also quantified. The experimental results showed that the sensor successfully measured chlorides concentration changes with good sensitivity. The sensor's response was not affected by temperature and humidity and showed good reversibility and stability. However, the pH of the pore solution affected the sensor's response to chlorides and a sensor calibration equation that considers pH is proposed. The characterization work presented herein provides a base for the development of such chloride sensing method, which can provide useful information for chloride diffusion models updating and health monitoring of the concrete structures subjected to sodium chloride.

* Corresponding author. E-mail address: bohuang@hnust.edu.cn (Bo Huang)
jqw@hnust.edu.cn (Jianqun wang) m.saafi@lancaster.ac.uk (Mohamed Saafi)

Keywords: Geopolymer cement; graphene; chloride sensor, electrochemical spectroscopy.

1. Introduction

Corrosion of reinforcing steel is one of the main causes of deterioration in concrete structures. Chlorides (Cl^-) penetration into concrete typically occurs when water containing sodium chloride (NaCl) diffuses into the concrete. When the chlorides level on the surface of the embedded steel rebars reaches a critical level, their corrosion starts. Excessive corrosion leads to internal stresses at the concrete-steel interface, causing cracking and delamination of the concrete cover, potentially reducing the load carrying capacity of the structure [1–4].

The chlorides threshold content at the rebar level depends on the properties of chloride ions diffusion in concrete, the surface chloride concentration and the pH of the pore solution [5–7]. Previous studies have shown that pitting of reinforcing steel occurs at chloride concentration thresholds between 5 and 200 mM/L for pH levels between 12 and 12.5 [8–10]. As such, chloride diffusion models are routinely used together with the surface chloride concentration to predict the chloride content at the rebar level [11] for durability analysis and service life prediction of the concrete structures.

There are several non-destructive techniques available for measuring the chlorides content in the reinforced concrete structures using different sensing technologies such as electrical resistivity [12,13], optical fibers [6,14,15] and Ag/AgCl chloride [16–18] sensors. However, when embedded in concrete, the accuracy of these techniques is strongly affected by the concrete's environment. For example, the methods used in [12,13] are sensitive to OH^- , humidity and temperature, thus it is essential to decouple the measurements from these effects. Similarly, optical fiber sensors exhibit measurement errors caused by temperature changes and mechanical deformation [19,20]. The performance of Ag/AgCl sensors is also affected by OH^- , temperature and the existence of bromide, which can be found in seawater [21]. Recently, composite-based sensors have been developed to measure chloride in concrete. Carbon

nanotube (CNT)-based thin films were used as a potential substitute for Ag/AgCl chloride sensors [22]. These thin films were designed to act as both working electrodes and sensors [22]. Experimental results showed that these sensors exhibit low detection limit, low sensitivity and highly susceptible to mechanical and chemical damage in concrete structures.

Other chlorides sensors in the form of conductive graphene/cement [23] and carbon nanotubes/cement [24] composites have also been developed that measure chloride based on the assumption that the conductive fillers form continuous conductive networks within the cement matrix, and their electrical properties are only affected by the chloride ions. However, achieving continuous conductive networks is extremely challenging as these conductive fillers cannot be dispersed effectively in the cementitious materials. Plain geopolymer-based cement sensors were also used to measure the chlorides in concrete structures [25,26], based on the change in their electrical properties. It is well-known that the OH^- , K^+ , Ca^{2+} and Na^+ ions in the pore solution, humidity and temperature strongly affect the bulk electrical properties of the cementitious composites. However, the interference of these measurands in chlorides monitoring was not investigated and the methodologies determining chlorides independently of these measurands were not discussed in [23–25]. Although other chemical species such as S^{2-} and SO_4^{2-} exist in the pore solution, their effect on the electrical properties needs further studies and evidence.

In this paper, we present a low-cost cementitious composite sensor for chloride monitoring in concrete structures. The sensor was manufactured and its response to the chlorides was characterized. The sensor's sensitivity, stability and reversibility, and the interference of alkalinity, temperature and humidity were also investigated.

2. Experimental program

2.1 Materials and sensor fabrication

Fig. 1 shows the layout of the chloride sensor. It consists of a chloride ion-selective functionalized graphene film (18 mm x 24 mm x 0.5 mm) deposited on tapered mortar support and protected by a porous geopolymers layer of approximately 2 mm in thickness. The sensor has a graphene active sensing area of 4 mm x 18 mm located in the middle. The chloride ion-selective film consists of amine-functionalized graphene nanoplatelets (NH_2/GNPs) purchased from CheaptubesTM, USA. The porous protective geopolymers layer was produced from class F fly ash and an alkaline solution. The alkaline solution consisted of potassium silicate solution ($\text{SiO}_2 = 26.6\%$, $\text{K}_2\text{O} = 30.7\%$ and $\text{H}_2\text{O} = 42.7\%$). The alkaline solution-to-fly ash (A/F) ratio was 0.55, resulting a porous mixture.

Mortar synthesized from Ordinary Portland Cement (OPC) type CEM I 52.5N and fine sand was used to manufacture the sensor's support. The steps of manufacturing the chlorides sensor are shown in Fig. 2a. The sensor's support was cast and cure for a 28 days, then the rest of the sensor was built according to Fig. 2. A copper mesh with electrical wires was also inserted into the geopolymers layer to form the electrodes of the sensor. The fabricated sensor, shown in Fig. 2b, was cured at 60 °C for 24 h and was then embedded in a normal concrete cube (100 mm x 100 mm x 100 mm) at a depth of 3 cm from the top surface as shown in Fig. 2c.

2.2. Working principle of the chloride sensor

Fig. 3 shows the working principle of the chloride sensor. The Na^+ and Cl^- ions diffuse through the porous protective geopolymers layer and interact with the functionalized graphene film. During this process, the positively charged functional groups on the graphene film attract the predominant negatively charged hydrated Cl^- ions and repel the positively charged hydrated Na^+ , K^+ and Ca^{2+} ions. The chloride monitoring can be achieved by measuring the changes in

the electrical impedance properties of the electrochemical double-layer-based chloride sensor, caused by the change in the chloride content in concrete. The electrical impedance properties of the sensor may also be affected by factors such as temperature and humidity, the negatively charged OH⁻ ions. As such, these factors' effects on the sensor's response were investigated independently in this paper.

2.3. Morphology and characterization of the sensor's response to chloride

The morphology of the graphene, protective geopolymers layer and graphene-geopolymer interface was examined with a scanning electron microscope (SEM). The effect of the chlorides on the sensor's response was characterized using the test setup shown in Fig. 4. The concrete cube with the embedded sensor was put in a glass container filled with NaCl solution with chloride concentrations of 0, 10, 20, 40, 60, 80 to 100 mM/L and the response of the sensor to each concentration was measured and characterized at room temperature using EIS.

2.4. Characterization of sensor's response to combined chlorides and OH

The experimental program was repeated to investigate the combined effect of the alkalinity presence and chlorides on the sensor's response. The concrete cube with the embedded sensor was placed in a glass container filled with a solution consisting of mixture of 70% NaCl solution and 30% sodium hydroxide solution. The concentrations of Cl⁻ were 10, 20, 40, 60 and 100 mM/L, and the pH levels of the sodium hydroxide solution with pH levels of 12, 13 and 14. The change in the electrical impedance properties of the sensor as a function of chloride concentration and pH were determined at room temperature.

2.5. Effect of temperature and humidity on the sensor's response

The sensor was subjected to different humidity levels and temperatures without being subjected to chlorides using a temperature and humidity controlled environmental chamber. The concrete cube was placed in the chamber and EIS measurements were carried out at -10°C,

-5°C , 5°C , 20°C and 35°C and humidity of about 40% to determine the electrical impedance properties of the sensor as a function of temperature. During heating, the environmental chamber was heated from -10°C to 30°C in 5°C and 10°C steps. The electrical impedance properties of the sensor as a function of humidity were determined.

2.6. Stability and reversibility of the sensor

The stability of the sensor was investigated by monitoring its electrical impedance properties over a period of 30 days. The concrete cube was put in a glass tub filled with a NaCl solution using different chloride concentrations. The EIS measurements were conducted when the sensor's signal output was stabilized and the electrical impedance properties as a function of time were determined at room temperature. The reversibility of the sensor was investigated through a wet-dry cycle regime. The concrete cube was put in a glass container filled with a NaCl solution using different chloride concentrations and EIS were conducted during the cycles.

3. Results and discussion

3.1. Morphology of the sensor's materials

Fig. 5a shows that the morphology feature of the graphene film is dominated by wrinkles and folds as a result of the graphene nanoplatelets processing. Fig. 5b shows the microstructure of the protective geopolymers layer after the geopolymers reaction completion at 60°C . Geopolymers reaction involves a chemical reaction between the dissolved silicates and aluminates in the highly alkaline environment, resulting in an aluminosilicate gel binder [27]. According to Fig. 5b, the microstructure of the geopolymers layer is heterogeneous in nature incorporating unreacted fly ash particles. This could be the result of variation in the properties of the fly ash particles (i.e., physical, chemical, and mineralogical properties). As Fig. 5c shown, a good bond between the aluminosilicate gel and graphene is observed without delamination.

3.2. Characterization of the sensor's response subjected to different chloride concentrations

Fig. 6a shows the Bode plot of the real, imaginary parts and complex of the impedance for a typical chloride sensor at room temperature prior to exposure to NaCl. This figure suggests that the electrical resistance mainly dominates the overall impedance of the sensor. At frequencies between 100 Hz and 100 kHz, the capacitance is significantly reduced, and the overall impedance becomes purely resistive with an average value of 15 k Ω .

Fig. 6b shows the Nyquist plot that both the size of the capacitive line (incomplete semicircle) and the bulk resistance (low intersection point) decreases as the chloride concentration increases. Due to the porous nature of the geopolymers layer, the ion diffusion (low frequency region) increases with increasing chloride concentrations. This leads to a gradual decrease of the charge transfer resistance of the graphene sensing film accompanied by a gradual change of electrochemical kinetics from charge-transfer control to diffusion control. At chloride concentrations between 60 and 100 mM, the Nyquist plots are mainly characterized by a diagonal diffusion line with a very small capacitive line.

The effect of chloride on the Bode plot of the sensor's real and imaginary parts is shown in Fig. 7a-b, respectively. This shows that the real impedance (bulk resistance) and the imaginary impedance (bulk capacitance) of the sensor decrease when the chloride concentration increases due to the decrease in the ionic charge-transfer resistance and the increase in the ionic diffusion within the geopolymers layer.

3.3. Equivalent circuit model for the sensor

The four in-series components of the equivalent circuit (EC) model representing the chloride sensor are shown in Fig. 8. In the EC model, the resistor R_1 represents the resistance of the electrical leads connecting the sensor to the EIS system. The resistance of the geopolymers matrix and the charge transfer resistance are also included and represented by R_2 and R_3 , respectively. The constant phase element CPE_1 simulates the capacitive effect in the sensor,

while the constant phase element CPE₂ simulates the double layer capacitance between the graphene sheets and the chloride ions. The Warburg diffusion element (W₁) represents the resistance of the ion diffusion in the system. The CPE and Warburg elements are generally described by their parameters in the following equivalent impedance equations.

$$Z_{CPE}(\omega) = \frac{1}{Q_0}(j\omega)^{-\alpha} \quad (3)$$

$$Z_W(\omega) = \frac{1}{Y_0\sqrt{j\omega}} \coth(B\sqrt{j\omega}) \quad (4)$$

Here Q₀ (s ^{α} /Ω) and α are the CPE frequency-independent parameters and when $\alpha = 1$, the system behaves as an ideal capacitor and the parameter Q₀ has units of capacitance. When $\alpha = 0$, the system behaves as an ideal resistor and the parameter Q₀ has the unit of resistance. Y₀ and B in Eq. (4) denotes the diffusion coefficients.

The components of the EC model shown in Fig. 8 were determined for each chloride concentration by fitting the experimental impedances using the simplex method to minimize the least squares difference fitting between the measured and predicted impedance. The fitted and measured impedances are compared in Fig. 9.

Fig. 10 plots α and Q₀ as a function of chloride concentration for CPE₁ and CPE₂. As shown in Fig. 10a, the parameter α of CPE₁ remains constant at approximately 0.45 for chloride concentrations between 0 and 100 mM. This implies that CPE₁ becomes Warburg impedance which describes the diffusion process in the porous geopolymers layer. This can be confirmed by the almost linear increase of the parameter Q₀ of CPE₁ by increasing the chloride concentration as a result of the increased diffusion in the geopolymers layer (Fig. 10b).

The effect of chloride concentrations on the diffusion coefficients (i.e., Warburg constants) is shown in Fig. 11a. As shown, the coefficients remain roughly constant until 40 mM before a sudden increase at 80 mM. This could be due to the increase in chloride

concentration, which triggers higher diffusion rate. The drop in the coefficients at 100 mM can be the result of the ions saturation at higher chloride concentrations [28]. From Fig. 11b, R_1 (the resistance of the electrodes/wiring, fluctuating around $100\ \Omega$) and R_2 (the resistance of the geopolymers layer around $100\ k\Omega$) are insensitive to chloride.

3.4. Sensor's sensitivity to combined chloride and hydroxide

Fig. 7 suggest that at the frequency of 1 kHz, the sensor works like a chemiresistor which is highly sensitive to chlorides. As such, the sensitivity of the sensor to chlorides and OH^- was determined at a frequency of 1 kHz. The relative change in resistance (ΔR) and phase shift ($\Delta\phi$) in response to chloride is shown in Fig. 12. As shown, bilinear and exponential relationships between the chlorides content and the electrical resistance of the sensor characterize the sensor's response. The bilinear response to the chlorides could be attributed to the formation of the Friedel's salt [29] where an anion-exchange mechanism takes place in the chlorides ranging between 10 to 30 mM. Because of this, the pH of the geopolymers pore solution is increased due to the release of OH^- ions from the AFm hydrates. As a result, the interference of OH^- ions is predominant in the 10 to 30 mM range due to their high electrical conductivity compared to the chloride ions.

Fig. 13 shows the effect of pH on the sensor's response to chloride. As can be seen, for a given chloride concentration, the electrical resistance of the sensor decreases as the pH of the pore solution increases. This is due to the accumulation of negatively charged OH^- ions on the positively charged graphene surface because of the electrostatic interaction, which increases the charge carrier density and mobility in the graphene, reducing the electrical resistance (real impedance) of the sensor. This means the sensor responds to both chloride and alkalinity of the pore solution. It is worth noting that the response of the sensor to OH^- is somewhat comparable to that of Ag/AgCl chloride sensors [30–32].

The experimental results shown in Fig. 13 were fitted to derive a relationship between the sensor's response and the chloride concentration. The non-linear curve lines of best fit and their equations are illustrated in Fig. 13. A general equation of the fitted lines can be expressed as:

$$Z' = -Z_0 Cl^- + Z_1(Cl^-)^2 + Z_2 \quad (5)$$

where Z' ($\text{k}\Omega$) is the real impedance of the sensor, and Z_0 ($\text{k}\Omega/\text{mM}$), Z_1 ($\text{k}\Omega/\text{mM}$) and Z_2 ($\text{k}\Omega$) are constants.

From Fig. 13, it can be observed that Z_0 (approximately 0.2 $\text{k}\Omega/\text{mM}$) and Z_1 (approximately 0.01 $\text{k}\Omega/\text{mM}$) remain constant over the entire pH range, whereas Z_2 is highly dependent on the pH level and decreases as the pH increases. Therefore, Z_2 represents the interference of the alkalinity of the pore solution. Once the sensor is calibrated, in-situ chloride contents can be measured according to Eq (5).

3.5. Stability and reversibility of the sensor

The stability of the chloride sensor in terms of the electrical resistance (real impedance) and phase shift at the chloride concentration of 60 mM is depicted in Fig. 14. As shown, the fluctuation of the sensor's outputs over time is very small, suggesting a good stability over 30 days. The electrical resistance output of the sensor shows a positive drift of 2.19 Ω/day , whereas the phase shift output of the sensor shows a negative drift of 0.0072 deg/day, which are very small compared to the measured sensitivities and their effect on the sensor's response to chlorides.

To confirm the reversibility, a typical wet-dry cycle when the chloride concentration is 40 mM is applied on the sensor. As can be seen in Fig. 15, the time taken to reach a steady output value from 0 mM (dry state) to 40 mM (wet state) is 8.5 min. This response time is much longer than that of the Ag/AgCl sensor studied in [29] in which it takes 1.5 minutes to reach a steady potential value from a chloride concentration of 1 mM to 1000 mM [29]. This

could be attributed to the slow diffusion of the chloride ions through the geopolymers layer. The time taken to reach a stable output is about 4.5 min and the time for the sensor to go back to its original state during drying is 11 min with a deviation of about 0.3%. These results indicate that the response time of the sensor during the wet-dry cycle is very high compared to the commonly used Ag/AgCl sensors [29]. The response time of the sensor can be improved by adjusting and optimizing the porosity structure of the geopolymers layer to allow faster diffusion and dehydration of the chloride ions without compromising its properties.

3.6. Effect of temperature and humidity

To elucidate whether the sensor output is affected by the environmental interferences resulting from the temperature and humidity exposure, the real impedance (bulk resistance) of the sensor was measured at different temperatures and humidity levels as shown in Fig. 16, respectively. In this study, the temperature and humidity interferences were studied independently and without the presence of NaCl and pore solution for easy decoupling. From Fig. 16a, it appears that the temperature range used in this study has little effect and no obvious trend on the sensor's response. This could be attributed to the low thermal conductivity of the geopolymers protective layer [33]. In addition, previous studies have shown that the electrical properties of graphene are insensitive to temperature within the range of -10 to 60°C [34]. Fig. 16b shows that the humidity has little effect on the sensor's response. This is because the electrical conductivity of water is much lower than that of graphene. The obtained results suggest that temperature and humidity interferences are insignificant and hence their decoupling from the chloride measurements is not required.

4. Conclusions

In this paper, we demonstrated the feasibility of monitoring the chlorides in concrete structures using a sensor consisting of functionalized graphene film sandwiched between geopolymers and OPC cementitious composites. The developed cementitious composite sensor

was coupled with EIS to measure its electrical impedance properties. An experimental program was carried out to characterize the performance of the sensor when subjected to chloride ions, humidity, temperature and alkalinity. The stability and reversibility of the sensor were characterized and an electric circuit model was used to gain a deep understanding of the sensor's electrical response to the chlorides. It was found that the sensor is highly sensitive to chlorides and exhibits a chemiresistive behaviour with a good stability and reversibility because of the interaction of chloride ions with the graphene sensing film. It was also found that the sensor is insensitive to humidity and temperature ranges found in a typical civil engineering environment. This means that chloride contents can be measured independently of these two environmental parameters. However, the sensor is highly sensitive to the alkalinity of the pore solution. Thus, a preliminary expression of the sensor response that considers the interference of alkalinity (OH^- ions) is proposed.

The chloride sensor prototype presented herein offers a cost-effective, easy-to-install and durable sensor system for health monitoring and management of the civil infrastructure subjected to chloride-induced corrosion. The sensors could be deployed in the form of a structural health monitoring system to continuously measure chloride contents in concrete. The information can be used to update the parameters of chloride diffusion models for the prediction of corrosion initiation, maintenance, and service-life performance of concrete structures.

Acknowledgments

The work is supported by the Scientific Research Found of Hunan provincial Education Department of China (22B0473), Royal Society (IEC\NSFC\191350), the National Natural Science Foundation of China, China (No. 52175112).

Figures

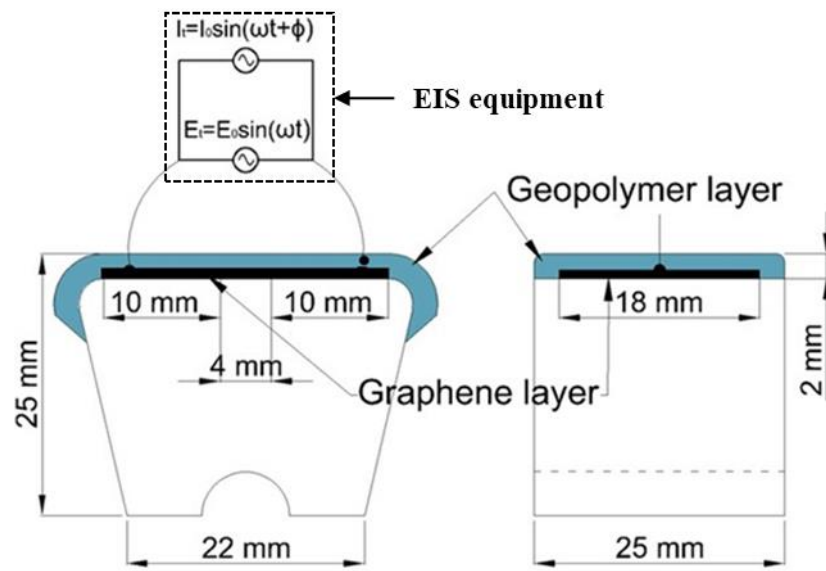


Fig. 1. Layout and size of the chloride sensor.

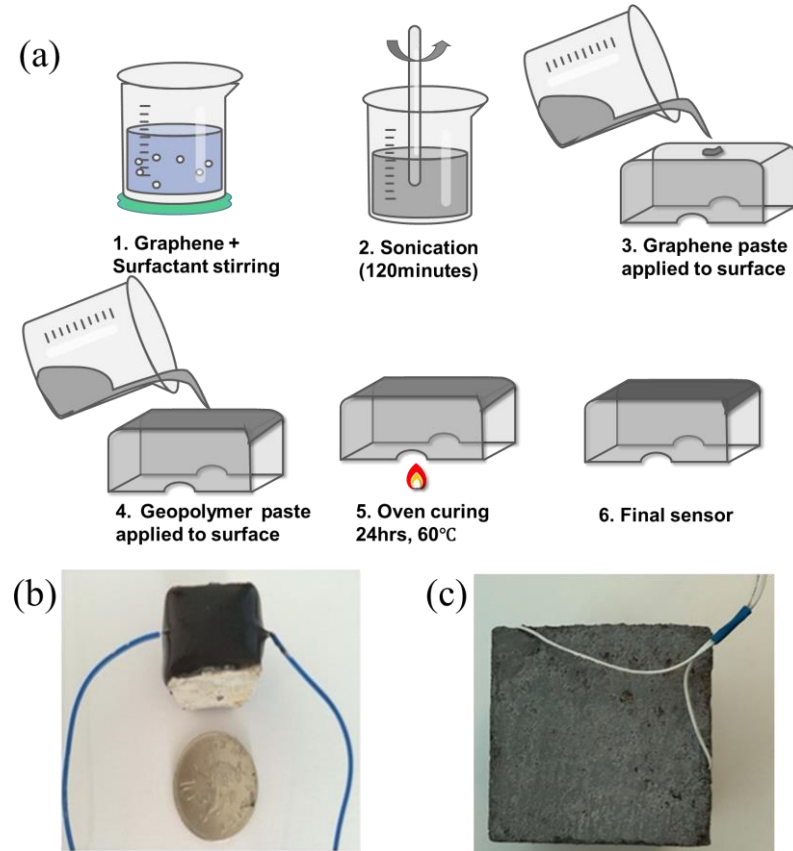


Fig. 2. Chloride sensor (a) manufacturing process, (b) completed chloride sensor, (c) concrete cube with the embedded sensor.

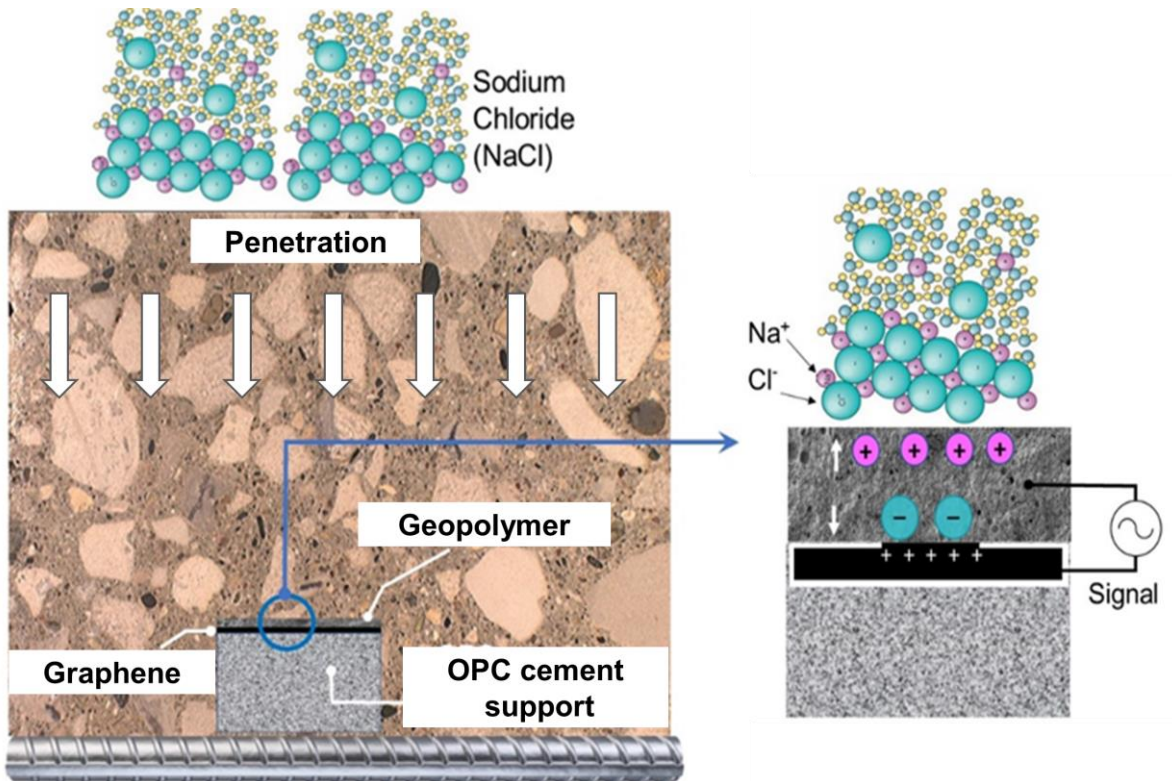


Fig. 3. Chloride sensor working principle.

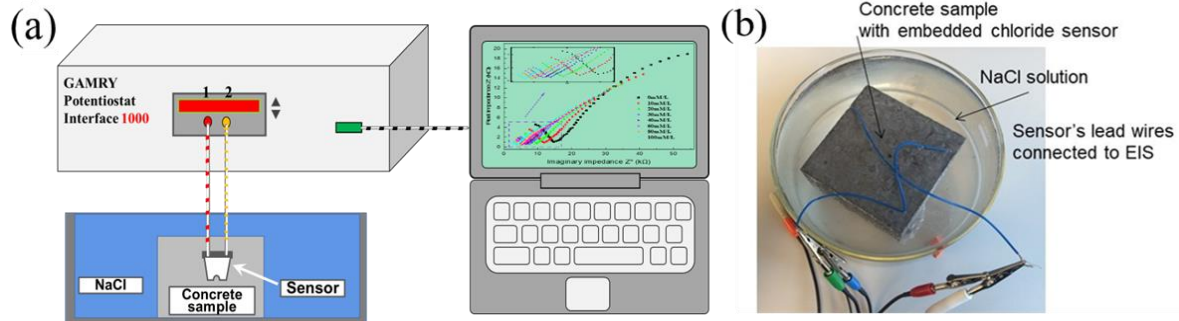


Fig. 4. Experimental test set up for the sensor subjected to NaCl solution.

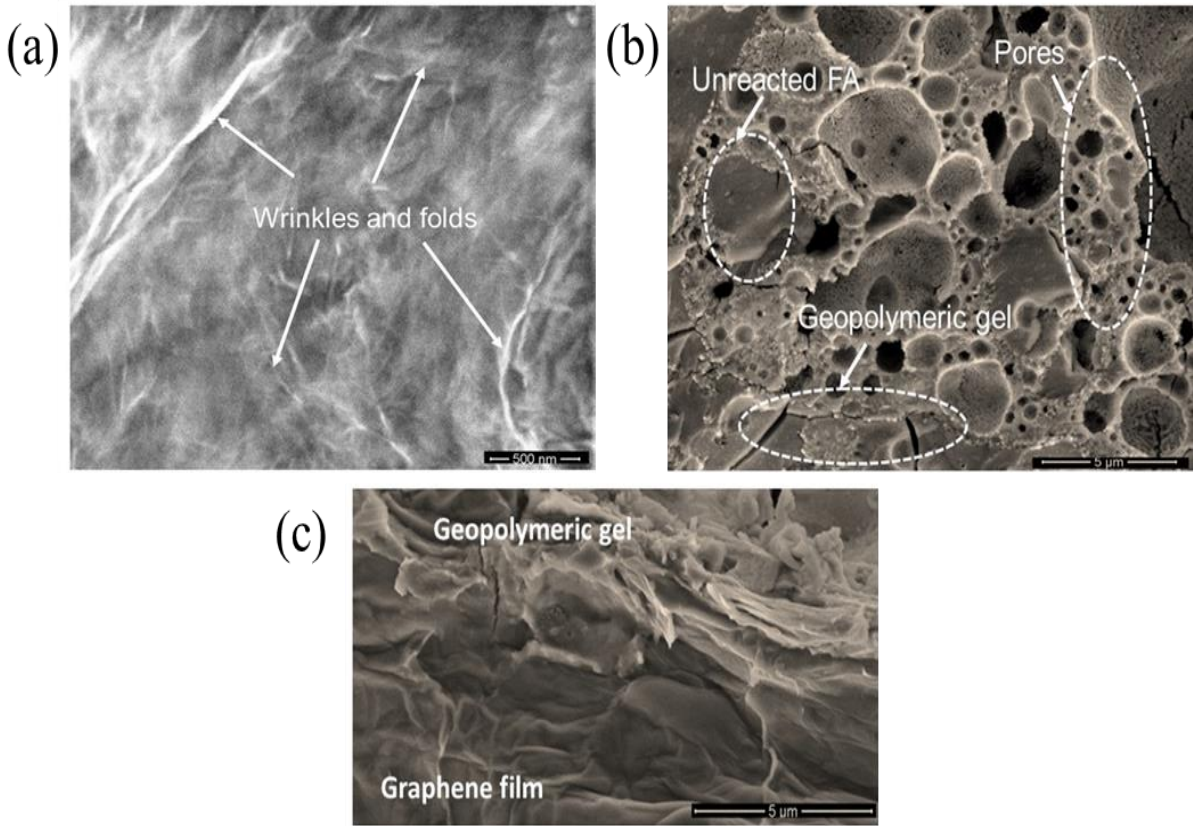


Fig. 5. SEM micro images of (a) Graphene film, (b) Geopolymer microstructure, (c) Geopolymer layer on the graphene film.

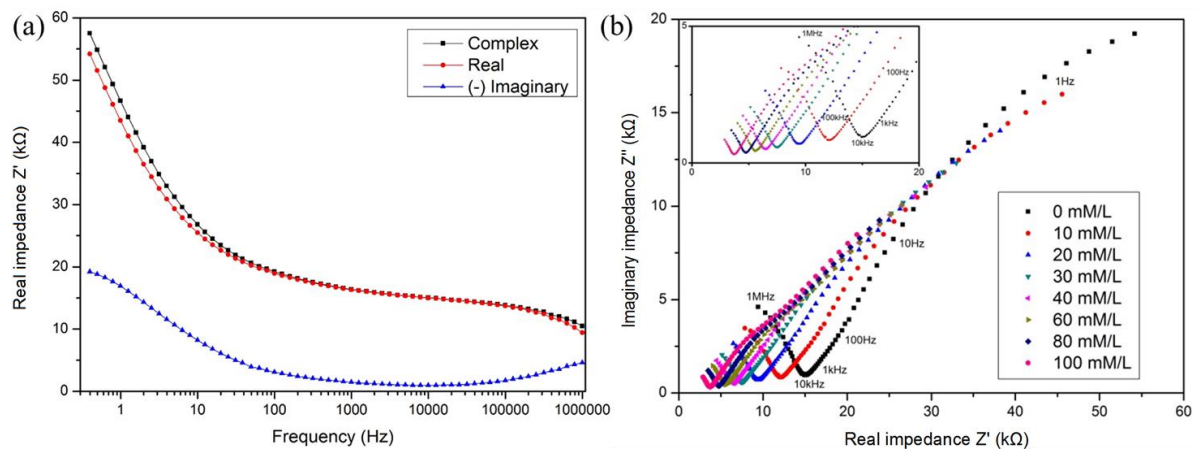


Fig. 6 Impedance of the sensor at room temperature (a) Bode plot prior exposure to chloride, (b) Nyquist plot at different Cl^- concentrations.

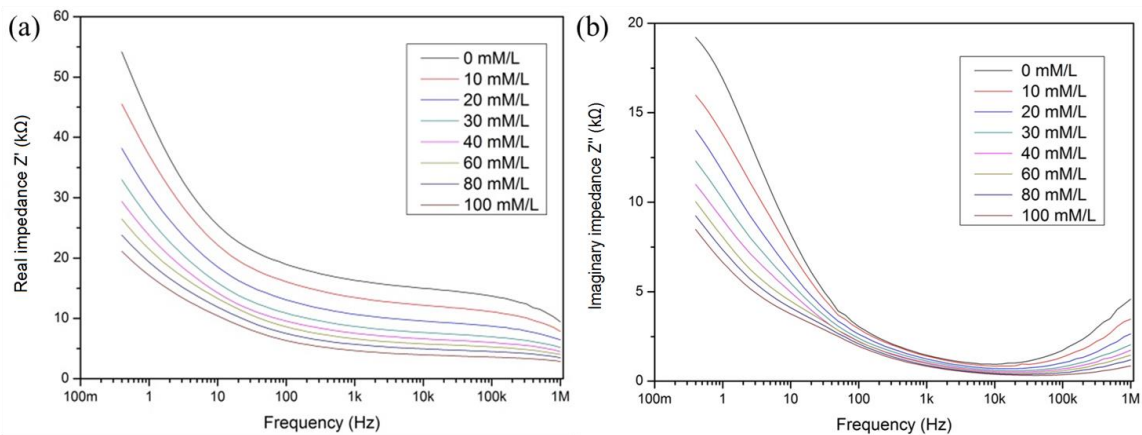


Fig. 7. Bode plot of the sensor at different Cl^- concentrations (a) real impedance, (b) imaginary impedance.

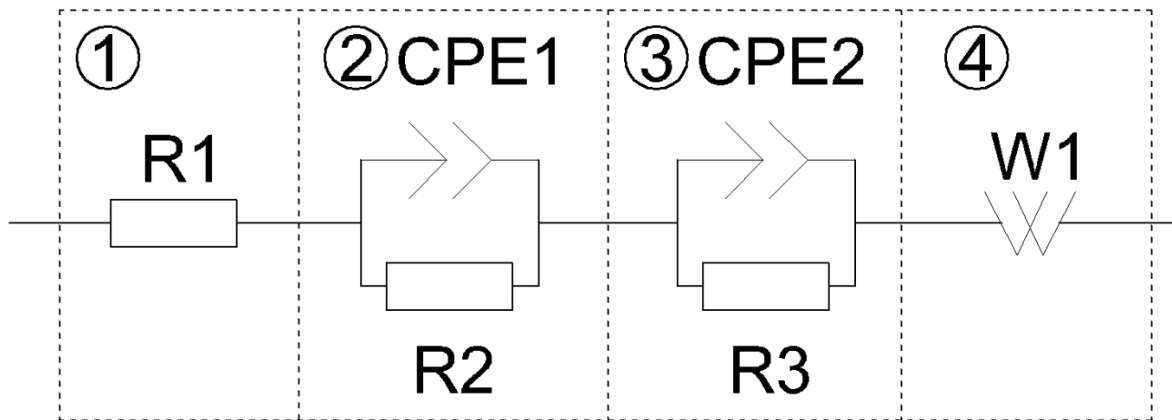


Fig. 8. Equivalent circuit for the sensor.

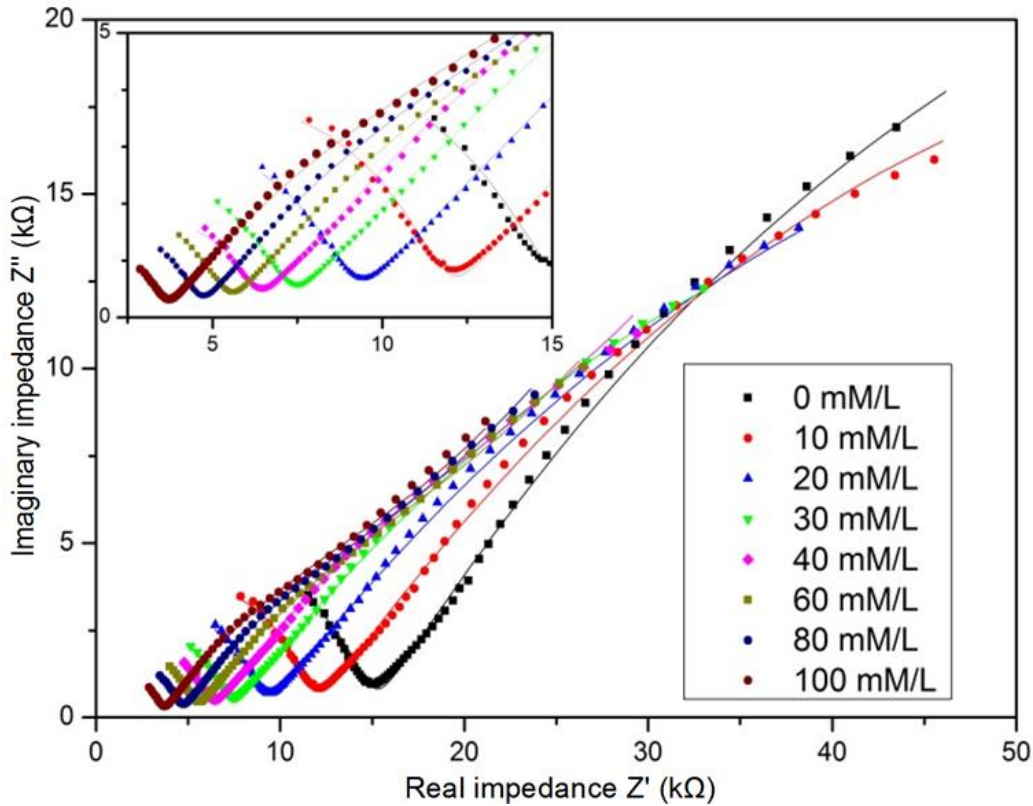


Fig. 9. Nyquist plots for the sensor at different Cl^- concentrations and the corresponding equivalent circuit (solid lines).

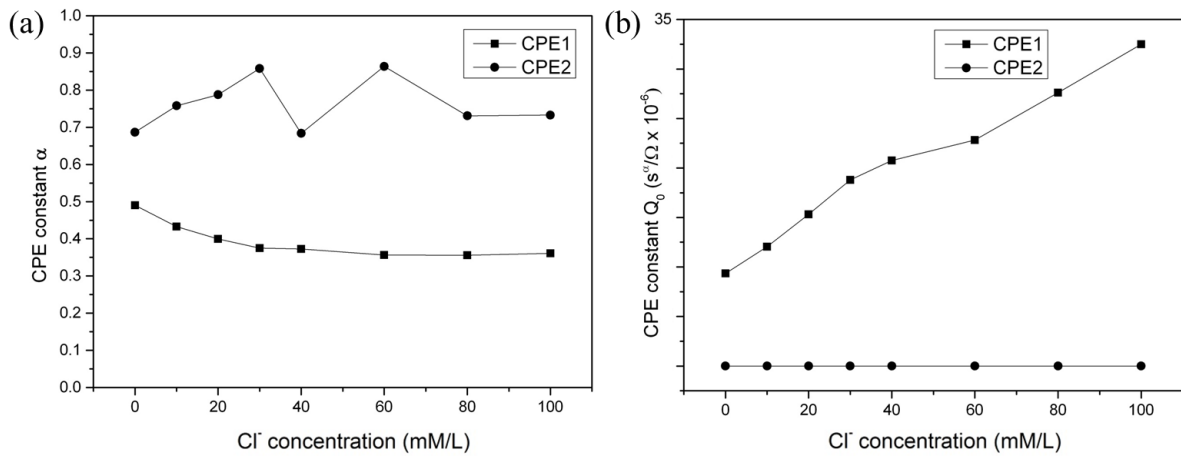


Fig. 10. Effect of Cl^- concentrations on the equivalent circuit parameters for the sensor (a) parameter α and (b) parameter Q_0 .

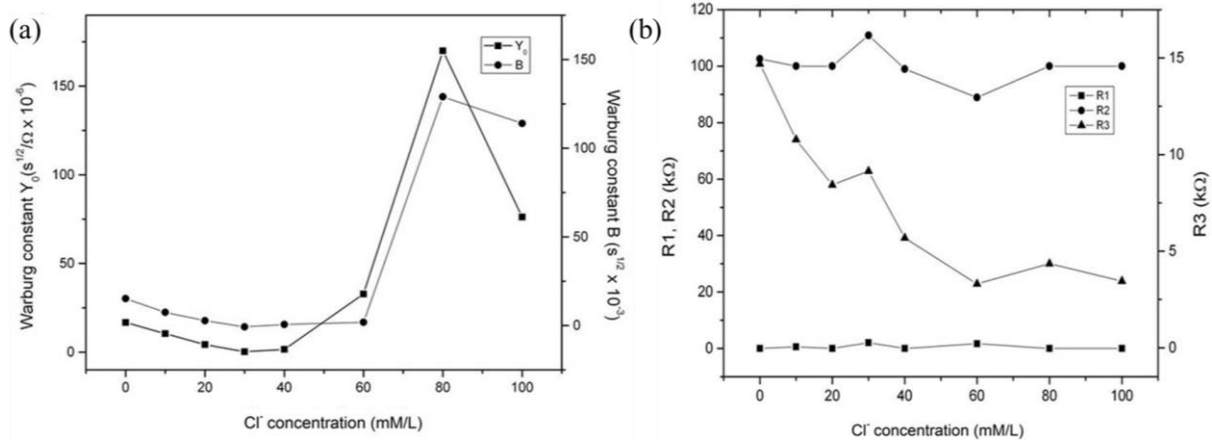


Fig. 11. Effect of Cl^- concentrations on the equivalent circuit parameters for the sensor (a) Warburg elements Y_0 and B , and (b) R_1 , R_2 and R_3 .

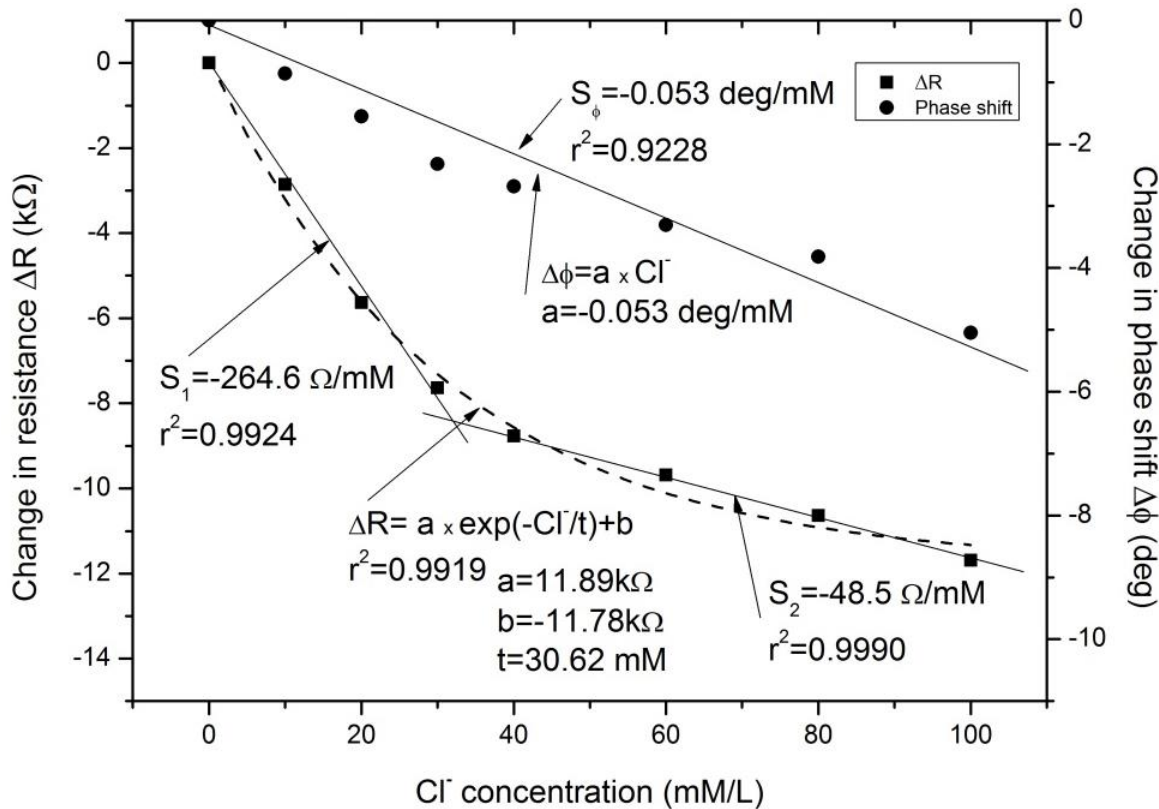


Fig. 12 Sensitivity of the sensor at 1 kHz.

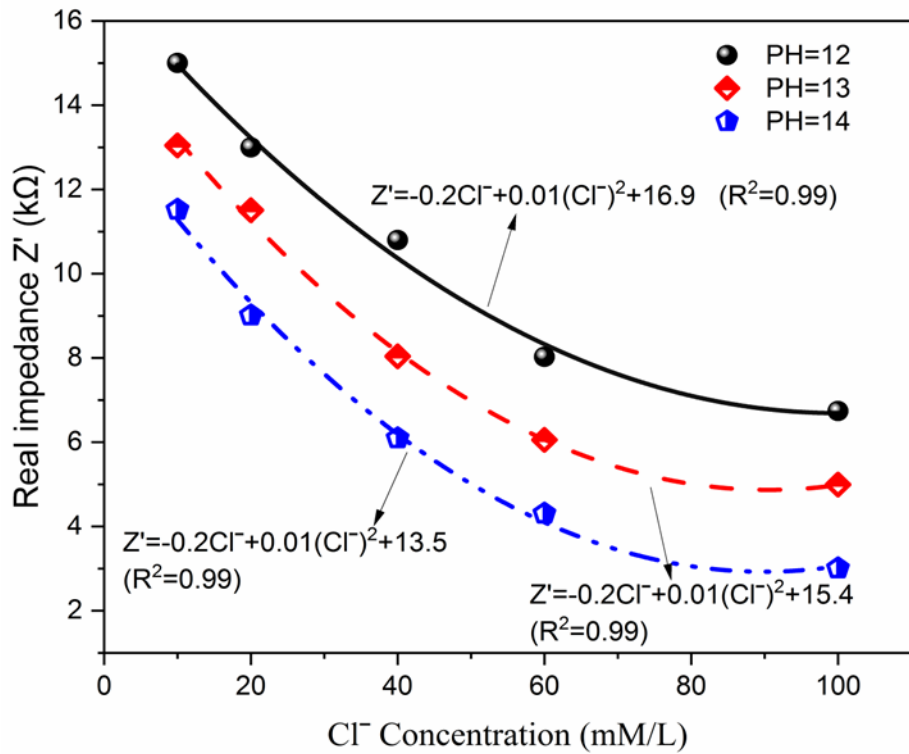


Fig. 13 Effect of pH on the response of the sensor at 1 kHz.

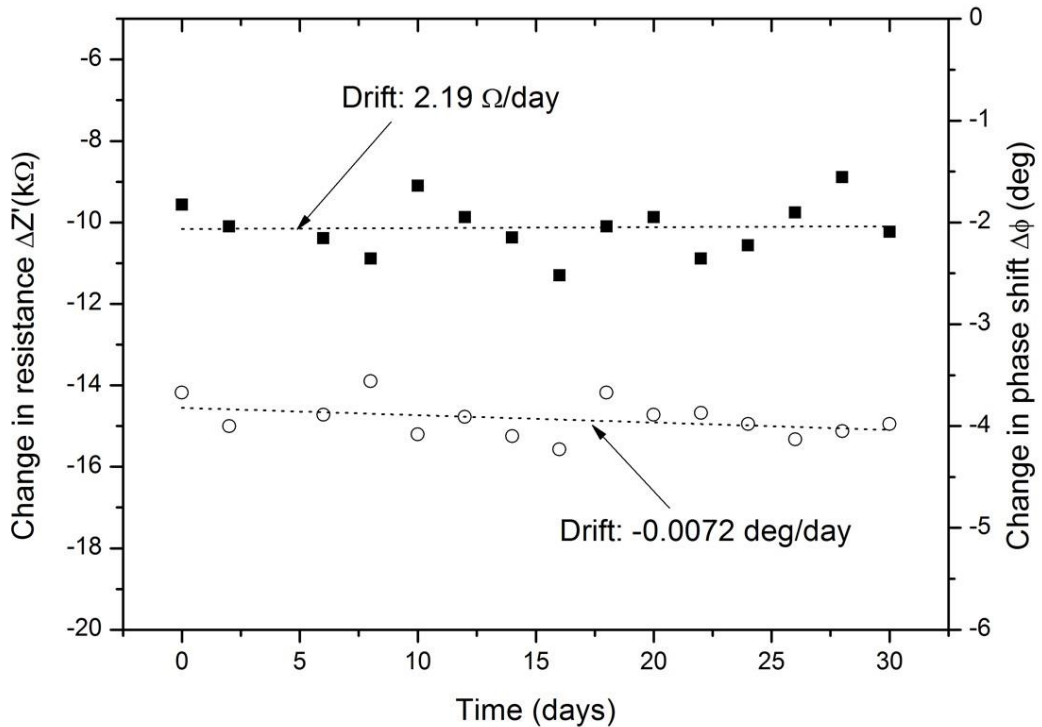


Fig. 14 Stability of the sensor at 1 kHz and 60 mM.

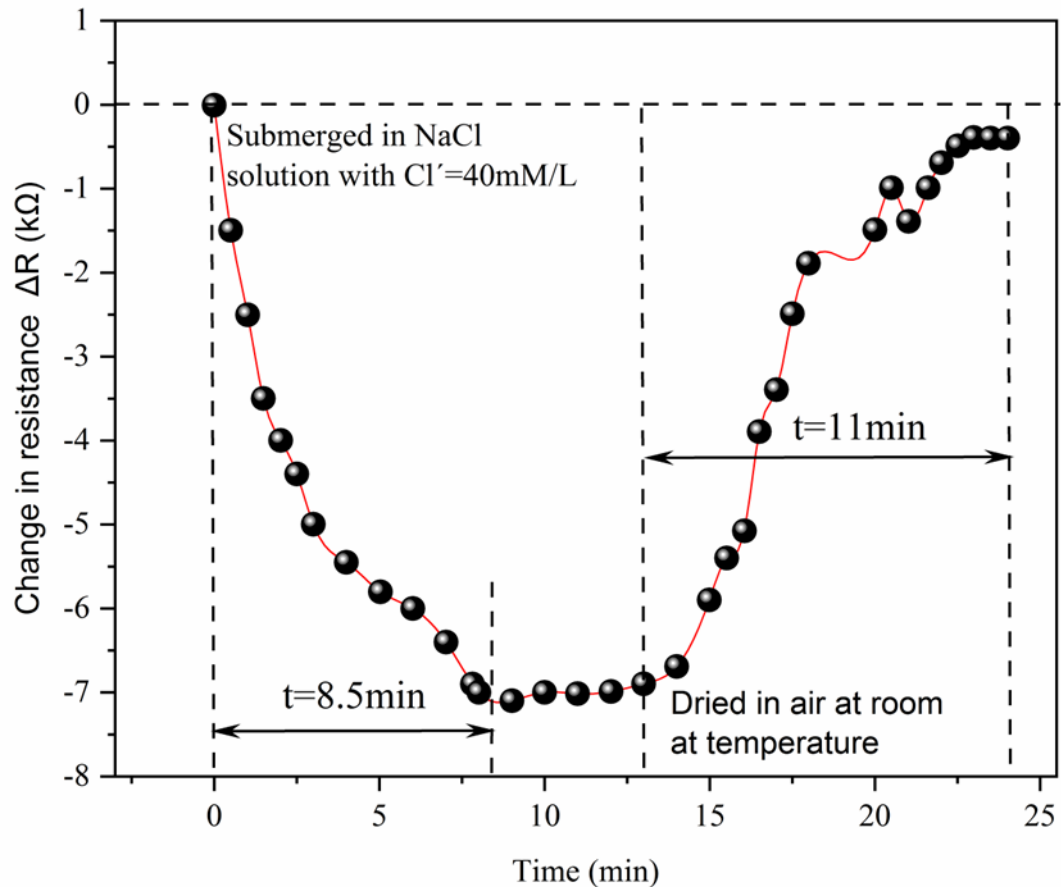


Fig. 15 Reversibility of the sensor under one wet-dry cycle at 1 kHz and 40 mM.

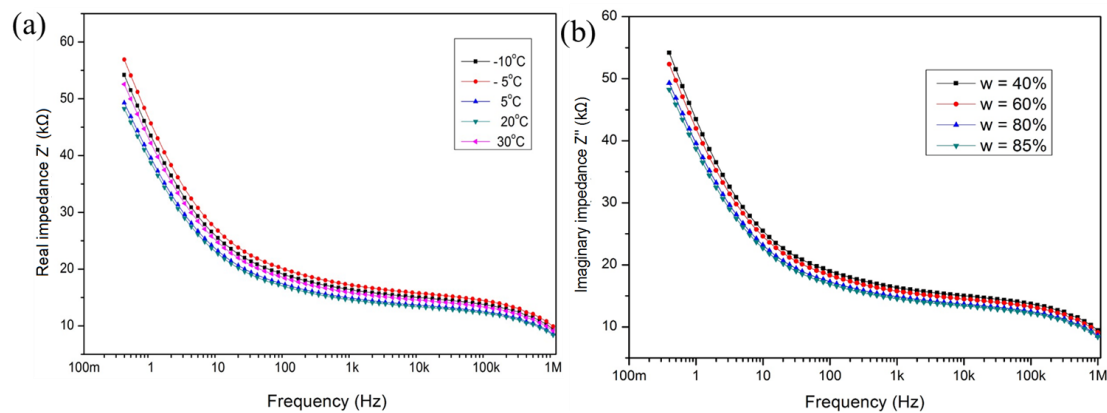


Fig. 16 Sensor at 1 kHz response effect of (a) temperature, (b) humidity.

Reference

- [1] S. Fang, L. Li, Z. Luo, Z. Fang, D. Huang, F. Liu, H. Wang, Z. Xiong, Novel FRP interlocking multi-spiral reinforced-seawater sea-sand concrete square columns with longitudinal hybrid FRP–steel bars: Monotonic and cyclic axial compressive behaviours, *Compos. Struct.* 305 (2023) 116487.
- [2] L. Yu, R. François, V.H. Dang, V. L'Hostis, R. Gagné, Development of chloride-induced corrosion in pre-cracked RC beams under sustained loading: Effect of load-induced cracks, concrete cover, and exposure conditions, *Cem. Concr. Res.* 67 (2015) 246–258. <https://doi.org/10.1016/j.cemconres.2014.10.007>.
- [3] S.P. Karthick, S. Muralidharan, V. Saraswathy, K. Thangavel, Long-term relative performance of embedded sensor and surface mounted electrode for corrosion monitoring of steel in concrete structures, *Sensors Actuators, B Chem.* 192 (2014) 303–309. <https://doi.org/10.1016/j.snb.2013.10.123>.
- [4] G. Zhang, C. Chen, K. Li, F. Xiao, J. Sun, Y. Wang, X. Wang, Multi-objective optimisation design for GFRP tendon reinforced cemented soil, *Constr. Build. Mater.* 320 (2022) 126297. <https://doi.org/10.1016/j.conbuildmat.2021.126297>.
- [5] K.Y. Ann, J.H. Ahn, J.S. Ryou, The importance of chloride content at the concrete surface in assessing the time to corrosion of steel in concrete structures, *Constr. Build. Mater.* 23 (2009) 239–245. <https://doi.org/10.1016/j.conbuildmat.2007.12.014>.
- [6] K.T. Wan, C.K.Y. Leung, L. Chen, A novel optical fiber sensor for steel corrosion in concrete structures, *Sensors.* 8 (2008) 1960–1976. <https://doi.org/10.3390/s8031960>.
- [7] Y.A. Villagrán-Zaccardi, C. Andrade, Chloride ingress rate and threshold content, as determined by the ‘Integral’ test method, in concrete with several w/c ratios in saturated and unsaturated conditions, *Dev. Built Environ.* 8 (2021). <https://doi.org/10.1016/j.dibe.2021.100062>.
- [8] J. Xu, L. Jiang, J. Wang, Influence of detection methods on chloride threshold value for the corrosion of steel reinforcement, *Constr. Build. Mater.* 23 (2009) 1902–1908. <https://doi.org/10.1016/j.conbuildmat.2008.09.011>.
- [9] H. An, G. Meng, Y. Wang, J. Wang, B. Liu, F. Wang, Study on the chloride threshold and risk assessment of rebar corrosion in simulated concrete pore solutions under applied potential, *Coatings.* 10 (2020). <https://doi.org/10.3390/COATINGS10050505>.
- [10] C.L. Page, N.R. Short, W.R. Holden, The influence of different cements on chloride-induced corrosion of reinforcing steel, *Cem. Concr. Res.* 16 (1986) 79–86.

[https://doi.org/10.1016/0008-8846\(86\)90071-2](https://doi.org/10.1016/0008-8846(86)90071-2).

- [11] K. Stanish, M. Thomas, The use of bulk diffusion tests to establish time-dependent concrete chloride diffusion coefficients, *Cem. Concr. Res.* 33 (2003) 55–62.
[https://doi.org/10.1016/S0008-8846\(02\)00925-0](https://doi.org/10.1016/S0008-8846(02)00925-0).
- [12] O.S. and O.E. Gjoryv, Electrical Resistivity Measurements for Quality Control During Concrete Construction, *ACI Mater. J.* 105 (n.d.). <https://doi.org/10.14359/20195>.
- [13] Y. Lecieux, F. Schoefs, S. Bonnet, T. Lecieux, S.P. Lopes, Quantification and uncertainty analysis of a structural monitoring device: Detection of chloride in concrete using DC electrical resistivity measurement, *Nondestruct. Test. Eval.* 30 (2015) 216–232. <https://doi.org/10.1080/10589759.2015.1029476>.
- [14] T.H. Nguyen, T. Venugopala, S. Chen, T. Sun, K.T.V. Grattan, S.E. Taylor, P.A.M. Basheer, A.E. Long, Fluorescence based fibre optic pH sensor for the pH 10-13 range suitable for corrosion monitoring in concrete structures, *Sensors Actuators, B Chem.* 191 (2014) 498–507. <https://doi.org/10.1016/j.snb.2013.09.072>.
- [15] P.L. Fuhr, D.R. Huston, Fiber optic chloride threshold detectors for concrete structures, *J. Struct. Control.* 7 (2000) 77–102.
- [16] G.S. Duffó, S.B. Farina, C.M. Giordano, Characterization of solid embeddable reference electrodes for corrosion monitoring in reinforced concrete structures, *Electrochim. Acta.* 54 (2009) 1010–1020.
<https://doi.org/10.1016/j.electacta.2008.08.025>.
- [17] M.A. Climent-Llorca, E. Viqueira-Pérez, M.M. López-Atalaya, Embeddable Ag/AgCl sensors for in-situ monitoring chloride contents in concrete, *Cem. Concr. Res.* 26 (1996) 1157–1161.
- [18] J.M. Gandía-Romero, R. Bataller, P. Monzón, I. Campos, E. García-Breijo, M. Valcuende, J. Soto, Characterization of embeddable potentiometric thick-film sensors for monitoring chloride penetration in concrete, *Sensors Actuators, B Chem.* 222 (2016) 407–418. <https://doi.org/10.1016/j.snb.2015.07.056>.
- [19] Z. Zhang, J. Hu, Y. Ma, Y. Wang, H. Huang, Z. Zhang, J. Wei, S. Yin, Q. Yu, A state-of-the-art review on Ag/AgCl ion-selective electrode used for non-destructive chloride detection in concrete, *Compos. Part B Eng.* 200 (2020) 108289.
<https://doi.org/10.1016/j.compositesb.2020.108289>.
- [20] T.H.T. Chan, L. Yu, H.Y. Tam, Y.Q. Ni, S.Y. Liu, W.H. Chung, L.K. Cheng, Fiber Bragg grating sensors for structural health monitoring of Tsing Ma bridge: Background and experimental observation, *Eng. Struct.* 28 (2006) 648–659.

<https://doi.org/10.1016/j.engstruct.2005.09.018>.

- [21] C.P. Atkins, M.A. Carter, J.D. Scantlebury, Sources of error in using silver/silver chloride electrodes to monitor chloride activity in concrete, *Cem. Concr. Res.* 31 (2001) 1207–1211. [https://doi.org/10.1016/S0008-8846\(01\)00544-0](https://doi.org/10.1016/S0008-8846(01)00544-0).
- [22] Y. Liu, J. Lynch, The development of chloride ion selective polypyrrole thin film on a layer-by-layer carbon nanotube working electrode, in: Proc.SPIE, 2011.
<https://doi.org/10.1117/12.880063>.
- [23] M. Jin, L. Jiang, M. Lu, S. Bai, Monitoring chloride ion penetration in concrete structure based on the conductivity of graphene/cement composite, *Constr. Build. Mater.* 136 (2017) 394–404. <https://doi.org/10.1016/j.conbuildmat.2017.01.054>.
- [24] H.K. Kim, Chloride penetration monitoring in reinforced concrete structure using carbon nanotube/cement composite, *Constr. Build. Mater.* 96 (2015) 29–36.
<https://doi.org/10.1016/j.conbuildmat.2015.07.190>.
- [25] L. Biondi, M. Perry, J. McAlorum, C. Vlachakis, A. Hamilton, G. Lo, Alkali-Activated Cement Sensors for Sodium Chloride Monitoring, *IEEE Sens. J.* 21 (2021) 21197–21204. <https://doi.org/10.1109/JSEN.2021.3100582>.
- [26] L. Biondi, M. Perry, J. McAlorum, C. Vlachakis, A. Hamilton, Geopolymer-based moisture sensors for reinforced concrete health monitoring, *Sensors Actuators, B Chem.* 309 (2020) 127775. <https://doi.org/10.1016/j.snb.2020.127775>.
- [27] A. Benhamouda, J. Castro-Gomes, Preliminary Study of the Rheological and Mechanical Properties of Alkali-activated Concrete Based on Tungsten Mining Waste Mud, *KnE Eng.* 2020 (2020) 101–110. <https://doi.org/10.18502/keg.v5i4.6801>.
- [28] A. Revil, D. Jougnot, Diffusion of ions in unsaturated porous materials, *J. Colloid Interface Sci.* 319 (2008) 226–235. <https://doi.org/10.1016/j.jcis.2007.10.041>.
- [29] S. Karthick, S.J. Kwon, H.S. Lee, S. Muralidharan, V. Saraswathy, R. Natarajan, Fabrication and evaluation of a highly durable and reliable chloride monitoring sensor for civil infrastructure, *RSC Adv.* 7 (2017) 31252–31263.
<https://doi.org/10.1039/c7ra05532c>.
- [30] M. Jin, L. Jiang, D. Tao, S. Bai, Characterization of Ag/AgCl electrode manufactured by immersion in sodium hypochlorite acid for monitoring chloride content in concrete, *Constr. Build. Mater.* 122 (2016) 310–319.
<https://doi.org/10.1016/j.conbuildmat.2016.05.163>.
- [31] G. De Vera, M.A. Climent, C. Antón, A. Hidalgo, C. Andrade, Determination of the selectivity coefficient of a chloride ion selective electrode in alkaline media simulating

- the cement paste pore solution, *J. Electroanal. Chem.* 639 (2010) 43–49.
- [32] Y.S. Femenias, U. Angst, F. Caruso, B. Elsener, Ag/AgCl ion-selective electrodes in neutral and alkaline environments containing interfering ions, *Mater. Struct.* 49 (2016) 2637–2651.
- [33] Z. Abdollahnejad, F. Pacheco-Torgal, T. Félix, W. Tahri, J. Barroso Aguiar, Mix design, properties and cost analysis of fly ash-based geopolymers foam, *Constr. Build. Mater.* 80 (2015) 18–30. <https://doi.org/10.1016/j.conbuildmat.2015.01.063>.
- [34] M. Tian, Y. Huang, W. Wang, R. Li, P. Liu, C. Liu, Y. Zhang, Temperature-dependent electrical properties of graphene nanoplatelets film dropped on flexible substrates, *J. Mater. Res.* 29 (2014) 1288–1294. <https://doi.org/10.1557/jmr.2014.109>.

Hybrid cement composite-based sensor for in-situ chloride monitoring in concrete structures

Bo Huang^{a,b*}, Jianqun Wang^{a*}, Gabor Piukovics^b, Niloufar Zabihi^b, Junjie Ye^c, Mohamed Saafi^{b*}, Jianqiao Ye^b

^aSchool of Civil Engineering, Hunan University of Science and Technology, Xiangtan, 411201, China

^bDepartment of Engineering, Lancaster University, Lancaster, LA1 4YR, UK

^cResearch Center for Applied Mechanics, Key Laboratory of Ministry of Education for Electronic Equipment Structure Design, Xidian University, Xi'an 710071, China

Abstract

In this paper, we present a rugged cementitious composite sensor for monitoring chloride ingress in concrete structures. The sensor is in the form of an electrochemical double-layer, consisting of a chloride ion-selective functionalized graphene film sandwiched between two cementitious composites. The cementitious composite chloride sensor was subjected to different chlorides concentrations and electrochemical impedance spectroscopy (EIS) measurements were conducted to characterize its response. The effect of the pore solution and the independent impact of temperature and humidity on the sensor's response were also quantified. The experimental results showed that the sensor successfully measured chlorides concentration changes with good sensitivity. The sensor's response was not affected by temperature and humidity and showed good reversibility and stability. However, the pH of the pore solution affected the sensor's response to chlorides and a sensor calibration equation that considers pH is proposed. The characterization work presented herein provides a base for the development of such chloride sensing method, which can provide useful information for chloride diffusion models updating and health monitoring of the concrete structures subjected to sodium chloride.

* Corresponding author. E-mail address: bohuang@hnust.edu.cn (Bo Huang)
jqw@hnust.edu.cn (Jianqun wang) m.saafi@lancaster.ac.uk (Mohamed Saafi)

Keywords: Geopolymer cement; graphene; chloride sensor, electrochemical spectroscopy.

1. Introduction

Corrosion of reinforcing steel is one of the main causes of deterioration in concrete structures. Chlorides (Cl^-) penetration into concrete typically occurs when water containing sodium chloride (NaCl) diffuses into the concrete. When the chlorides level on the surface of the embedded steel rebars reaches a critical level, their corrosion starts. Excessive corrosion leads to internal stresses at the concrete-steel interface, causing cracking and delamination of the concrete cover, potentially reducing the load carrying capacity of the structure [1–4].

The chlorides threshold content at the rebar level depends on the properties of chloride ions diffusion in concrete, the surface chloride concentration and the pH of the pore solution [5–7]. Previous studies have shown that pitting of reinforcing steel occurs at chloride concentration thresholds between 5 and 200 mM/L for pH levels between 12 and 12.5 [8–10]. As such, chloride diffusion models are routinely used together with the surface chloride concentration to predict the chloride content at the rebar level [11] for durability analysis and service life prediction of the concrete structures.

There are several non-destructive techniques available for measuring the chlorides content in the reinforced concrete structures using different sensing technologies such as electrical resistivity [12,13], optical fibers [6,14,15] and Ag/AgCl chloride [16–18] sensors. However, when embedded in concrete, the accuracy of these techniques is strongly affected by the concrete's environment. For example, the methods used in [12,13] are sensitive to OH^- , humidity and temperature, thus it is essential to decouple the measurements from these effects. Similarly, optical fiber sensors exhibit measurement errors caused by temperature changes and mechanical deformation [19,20]. The performance of Ag/AgCl sensors is also affected by OH^- , temperature and the existence of bromide, which can be found in seawater [21]. Recently, composite-based sensors have been developed to measure chloride in concrete. Carbon

nanotube (CNT)-based thin films were used as a potential substitute for Ag/AgCl chloride sensors [22]. These thin films were designed to act as both working electrodes and sensors [22]. Experimental results showed that these sensors exhibit low detection limit, low sensitivity and highly susceptible to mechanical and chemical damage in concrete structures.

Other chlorides sensors in the form of conductive graphene/cement [23] and carbon nanotubes/cement [24] composites have also been developed that measure chloride based on the assumption that the conductive fillers form continuous conductive networks within the cement matrix, and their electrical properties are only affected by the chloride ions. However, achieving continuous conductive networks is extremely challenging as these conductive fillers cannot be dispersed effectively in the cementitious materials. Plain geopolymer-based cement sensors were also used to measure the chlorides in concrete structures [25,26], based on the change in their electrical properties. It is well-known that the OH^- , K^+ , Ca^{2+} and Na^+ ions in the pore solution, humidity and temperature strongly affect the bulk electrical properties of the cementitious composites. However, the interference of these measurands in chlorides monitoring was not investigated and the methodologies determining chlorides independently of these measurands were not discussed in [23–25]. Although other chemical species such as S^{2-} and SO_4^{2-} exist in the pore solution, their effect on the electrical properties needs further studies and evidence.

In this paper, we present a low-cost cementitious composite sensor for chloride monitoring in concrete structures. The sensor was manufactured and its response to the chlorides was characterized. The sensor's sensitivity, stability and reversibility, and the interference of alkalinity, temperature and humidity were also investigated.

2. Experimental program

2.1 Materials and sensor fabrication

Fig. 1 shows the layout of the chloride sensor. It consists of a chloride ion-selective functionalized graphene film (18 mm x 24 mm x 0.5 mm) deposited on tapered mortar support and protected by a porous geopolymers layer of approximately 2 mm in thickness. The sensor has a graphene active sensing area of 4 mm x 18 mm located in the middle. The chloride ion-selective film consists of amine-functionalized graphene nanoplatelets (NH_2/GNPs) purchased from CheaptubesTM, USA. The porous protective geopolymers layer was produced from class F fly ash and an alkaline solution. The alkaline solution consisted of potassium silicate solution ($\text{SiO}_2 = 26.6\%$, $\text{K}_2\text{O} = 30.7\%$ and $\text{H}_2\text{O} = 42.7\%$). The alkaline solution-to-fly ash (A/F) ratio was 0.55, resulting a porous mixture.

Mortar synthesized from Ordinary Portland Cement (OPC) type CEM I 52.5N and fine sand was used to manufacture the sensor's support. The steps of manufacturing the chlorides sensor are shown in Fig. 2a. The sensor's support was cast and cure for a 28 days, then the rest of the sensor was built according to Fig. 2. A copper mesh with electrical wires was also inserted into the geopolymers layer to form the electrodes of the sensor. The fabricated sensor, shown in Fig. 2b, was cured at 60 °C for 24 h and was then embedded in a normal concrete cube (100 mm x 100 mm x 100 mm) at a depth of 3 cm from the top surface as shown in Fig. 2c.

2.2. Working principle of the chloride sensor

Fig. 3 shows the working principle of the chloride sensor. [The \$\text{Na}^+\$ and \$\text{Cl}^-\$ ions diffuse through the porous protective geopolymers layer and interact with the functionalized graphene film.](#) During this process, the positively charged functional groups on the graphene film attract the predominant negatively charged hydrated Cl^- ions and repel the positively charged hydrated Na^+ , K^+ and Ca^{2+} ions. The chloride monitoring can be achieved by measuring the changes in

the electrical impedance properties of the electrochemical double-layer-based chloride sensor, caused by the change in the chloride content in concrete. The electrical impedance properties of the sensor may also be affected by factors such as temperature and humidity, the negatively charged OH⁻ ions. As such, these factors' effects on the sensor's response were investigated independently in this paper.

2.3. Morphology and characterization of the sensor's response to chloride

The morphology of the graphene, protective geopolymers layer and graphene-geopolymer interface was examined with a scanning electron microscope (SEM). The effect of the chlorides on the sensor's response was characterized using the test setup shown in Fig. 4. The concrete cube with the embedded sensor was put in a glass container filled with NaCl solution with chloride concentrations of 0, 10, 20, 40, 60, 80 to 100 mM/L and the response of the sensor to each concentration was measured and characterized at room temperature using EIS.

2.4. Characterization of sensor's response to combined chlorides and OH

The experimental program was repeated to investigate the combined effect of the alkalinity presence and chlorides on the sensor's response. The concrete cube with the embedded sensor was placed in a glass container filled with a solution consisting of mixture of 70% NaCl solution and 30% sodium hydroxide solution. The concentrations of Cl⁻ were 10, 20, 40, 60 and 100 mM/L, and the pH levels of the sodium hydroxide solution with pH levels of 12, 13 and 14. The change in the electrical impedance properties of the sensor as a function of chloride concentration and pH were determined at room temperature.

2.5. Effect of temperature and humidity on the sensor's response

The sensor was subjected to different humidity levels and temperatures without being subjected to chlorides using a temperature and humidity controlled environmental chamber. The concrete cube was placed in the chamber and EIS measurements were carried out at -10°C,

-5°C , 5°C , 20°C and 35°C and humidity of about 40% to determine the electrical impedance properties of the sensor as a function of temperature. During heating, the environmental chamber was heated from -10°C to 30°C in 5°C and 10°C steps. The electrical impedance properties of the sensor as a function of humidity were determined.

2.6. Stability and reversibility of the sensor

The stability of the sensor was investigated by monitoring its electrical impedance properties over a period of 30 days. The concrete cube was put in a glass tub filled with a NaCl solution using different chloride concentrations. The EIS measurements were conducted when the sensor's signal output was stabilized and the electrical impedance properties as a function of time were determined at room temperature. The reversibility of the sensor was investigated through a wet-dry cycle regime. The concrete cube was put in a glass container filled with a NaCl solution using different chloride concentrations and EIS were conducted during the cycles.

3. Results and discussion

3.1. Morphology of the sensor's materials

Fig. 5a shows that the morphology feature of the graphene film is dominated by wrinkles and folds as a result of the graphene nanoplatelets processing. Fig. 5b shows the microstructure of the protective geopolymers layer after the geopolymers reaction completion at 60°C . Geopolymers reaction involves a chemical reaction between the dissolved silicates and aluminates in the highly alkaline environment, resulting in an aluminosilicate gel binder [27]. According to Fig. 5b, the microstructure of the geopolymers layer is heterogeneous in nature incorporating unreacted fly ash particles. This could be the result of variation in the properties of the fly ash particles (i.e., physical, chemical, and mineralogical properties). As Fig. 5c shown, a good bond between the aluminosilicate gel and graphene is observed without delamination.

3.2. Characterization of the sensor's response subjected to different chloride concentrations

Fig. 6a shows the Bode plot of the real, imaginary parts and complex of the impedance for a typical chloride sensor at room temperature prior to exposure to NaCl. This figure suggests that the electrical resistance mainly dominates the overall impedance of the sensor. At frequencies between 100 Hz and 100 kHz, the capacitance is significantly reduced, and the overall impedance becomes purely resistive with an average value of 15 k Ω .

Fig. 6b shows the Nyquist plot that both the size of the capacitive line (incomplete semicircle) and the bulk resistance (low intersection point) decreases as the chloride concentration increases. Due to the porous nature of the geopolymers layer, the ion diffusion (low frequency region) increases with increasing chloride concentrations. This leads to a gradual decrease of the charge transfer resistance of the graphene sensing film accompanied by a gradual change of electrochemical kinetics from charge-transfer control to diffusion control. At chloride concentrations between 60 and 100 mM, the Nyquist plots are mainly characterized by a diagonal diffusion line with a very small capacitive line.

The effect of chloride on the Bode plot of the sensor's real and imaginary parts is shown in Fig. 7a-b, respectively. This shows that the real impedance (bulk resistance) and the imaginary impedance (bulk capacitance) of the sensor decrease when the chloride concentration increases due to the decrease in the ionic charge-transfer resistance and the increase in the ionic diffusion within the geopolymers layer.

3.3. Equivalent circuit model for the sensor

The four in-series components of the equivalent circuit (EC) model representing the chloride sensor are shown in Fig. 8. In the EC model, the resistor R_1 represents the resistance of the electrical leads connecting the sensor to the EIS system. The resistance of the geopolymers matrix and the charge transfer resistance are also included and represented by R_2 and R_3 , respectively. The constant phase element CPE_1 simulates the capacitive effect in the sensor,

while the constant phase element CPE₂ simulates the double layer capacitance between the graphene sheets and the chloride ions. The Warburg diffusion element (W₁) represents the resistance of the ion diffusion in the system. The CPE and Warburg elements are generally described by their parameters in the following equivalent impedance equations.

$$Z_{CPE}(\omega) = \frac{1}{Q_0}(j\omega)^{-\alpha} \quad (3)$$

$$Z_W(\omega) = \frac{1}{Y_0\sqrt{j\omega}} \coth(B\sqrt{j\omega}) \quad (4)$$

Here Q₀ (s ^{α} /Ω) and α are the CPE frequency-independent parameters and when $\alpha = 1$, the system behaves as an ideal capacitor and the parameter Q₀ has units of capacitance. When $\alpha = 0$, the system behaves as an ideal resistor and the parameter Q₀ has the unit of resistance. Y₀ and B in Eq. (4) denotes the diffusion coefficients.

The components of the EC model shown in Fig. 8 were determined for each chloride concentration by fitting the experimental impedances using the simplex method to minimize the least squares difference fitting between the measured and predicted impedance. The fitted and measured impedances are compared in Fig. 9.

Fig. 10 plots α and Q₀ as a function of chloride concentration for CPE₁ and CPE₂. As shown in Fig. 10a, the parameter α of CPE₁ remains constant at approximately 0.45 for chloride concentrations between 0 and 100 mM. This implies that CPE₁ becomes Warburg impedance which describes the diffusion process in the porous geopolymers layer. This can be confirmed by the almost linear increase of the parameter Q₀ of CPE₁ by increasing the chloride concentration as a result of the increased diffusion in the geopolymers layer (Fig. 10b).

The effect of chloride concentrations on the diffusion coefficients (i.e., Warburg constants) is shown in Fig. 11a. As shown, the coefficients remain roughly constant until 40 mM before a sudden increase at 80 mM. This could be due to the increase in chloride

concentration, which triggers higher diffusion rate. The drop in the coefficients at 100 mM can be the result of the ions saturation at higher chloride concentrations [28]. From Fig. 11b, R_1 (the resistance of the electrodes/wiring, fluctuating around $100\ \Omega$) and R_2 (the resistance of the geopolymers layer around $100\ k\Omega$) are insensitive to chloride.

3.4. Sensor's sensitivity to combined chloride and hydroxide

Fig. 7 suggest that at the frequency of 1 kHz, the sensor works like a chemiresistor which is highly sensitive to chlorides. As such, the sensitivity of the sensor to chlorides and OH^- was determined at a frequency of 1 kHz. The relative change in resistance (ΔR) and phase shift ($\Delta\phi$) in response to chloride is shown in Fig. 12. As shown, bilinear and exponential relationships between the chlorides content and the electrical resistance of the sensor characterize the sensor's response. The bilinear response to the chlorides could be attributed to the formation of the Friedel's salt [29] where an anion-exchange mechanism takes place in the chlorides ranging between 10 to 30 mM. Because of this, the pH of the geopolymers pore solution is increased due to the release of OH^- ions from the AFm hydrates. As a result, the interference of OH^- ions is predominant in the 10 to 30 mM range due to their high electrical conductivity compared to the chloride ions.

Fig. 13 shows the effect of pH on the sensor's response to chloride. As can be seen, for a given chloride concentration, the electrical resistance of the sensor decreases as the pH of the pore solution increases. This is due to the accumulation of negatively charged OH^- ions on the positively charged graphene surface because of the electrostatic interaction, which increases the charge carrier density and mobility in the graphene, reducing the electrical resistance (real impedance) of the sensor. This means the sensor responds to both chloride and alkalinity of the pore solution. It is worth noting that the response of the sensor to OH^- is somewhat comparable to that of Ag/AgCl chloride sensors [30–32].

The experimental results shown in Fig. 13 were fitted to derive a relationship between the sensor's response and the chloride concentration. The non-linear curve lines of best fit and their equations are illustrated in Fig. 13. A general equation of the fitted lines can be expressed as:

$$Z' = -Z_0 Cl^- + Z_1(Cl^-)^2 + Z_2 \quad (5)$$

where Z' ($\text{k}\Omega$) is the real impedance of the sensor, and Z_0 ($\text{k}\Omega/\text{mM}$), Z_1 ($\text{k}\Omega/\text{mM}$) and Z_2 ($\text{k}\Omega$) are constants.

From Fig. 13, it can be observed that Z_0 (approximately 0.2 $\text{k}\Omega/\text{mM}$) and Z_1 (approximately 0.01 $\text{k}\Omega/\text{mM}$) remain constant over the entire pH range, whereas Z_2 is highly dependent on the pH level and decreases as the pH increases. Therefore, Z_2 represents the interference of the alkalinity of the pore solution. Once the sensor is calibrated, in-situ chloride contents can be measured according to Eq (5).

3.5. Stability and reversibility of the sensor

The stability of the chloride sensor in terms of the electrical resistance (real impedance) and phase shift at the chloride concentration of 60 mM is depicted in Fig. 14. As shown, the fluctuation of the sensor's outputs over time is very small, suggesting a good stability over 30 days. The electrical resistance output of the sensor shows a positive drift of 2.19 Ω/day , whereas the phase shift output of the sensor shows a negative drift of 0.0072 deg/day, which are very small compared to the measured sensitivities and their effect on the sensor's response to chlorides.

To confirm the reversibility, a typical wet-dry cycle when the chloride concentration is 40 mM is applied on the sensor. As can be seen in Fig. 15, the time taken to reach a steady output value from 0 mM (dry state) to 40 mM (wet state) is 8.5 min. This response time is much longer than that of the Ag/AgCl sensor studied in [29] in which it takes 1.5 minutes to reach a steady potential value from a chloride concentration of 1 mM to 1000 mM [29]. This

could be attributed to the slow diffusion of the chloride ions through the geopolymers layer. The time taken to reach a stable output is about 4.5 min and the time for the sensor to go back to its original state during drying is 11 min with a deviation of about 0.3%. These results indicate that the response time of the sensor during the wet-dry cycle is very high compared to the commonly used Ag/AgCl sensors [29]. The response time of the sensor can be improved by adjusting and optimizing the porosity structure of the geopolymers layer to allow faster diffusion and dehydration of the chloride ions without compromising its properties.

3.6. Effect of temperature and humidity

To elucidate whether the sensor output is affected by the environmental interferences resulting from the temperature and humidity exposure, the real impedance (bulk resistance) of the sensor was measured at different temperatures and humidity levels as shown in Fig. 16, respectively. In this study, the temperature and humidity interferences were studied independently and without the presence of NaCl and pore solution for easy decoupling. From Fig. 16a, it appears that the temperature range used in this study has little effect and no obvious trend on the sensor's response. This could be attributed to the low thermal conductivity of the geopolymers protective layer [33]. In addition, previous studies have shown that the electrical properties of graphene are insensitive to temperature within the range of -10 to 60°C [34]. Fig. 16b shows that the humidity has little effect on the sensor's response. This is because the electrical conductivity of water is much lower than that of graphene. The obtained results suggest that temperature and humidity interferences are insignificant and hence their decoupling from the chloride measurements is not required.

4. Conclusions

In this paper, we demonstrated the feasibility of monitoring the chlorides in concrete structures using a sensor consisting of functionalized graphene film sandwiched between geopolymers and OPC cementitious composites. The developed cementitious composite sensor

was coupled with EIS to measure its electrical impedance properties. An experimental program was carried out to characterize the performance of the sensor when subjected to chloride ions, humidity, temperature and alkalinity. The stability and reversibility of the sensor were characterized and an electric circuit model was used to gain a deep understanding of the sensor's electrical response to the chlorides. It was found that the sensor is highly sensitive to chlorides and exhibits a chemiresistive behaviour with a good stability and reversibility because of the interaction of chloride ions with the graphene sensing film. It was also found that the sensor is insensitive to humidity and temperature ranges found in a typical civil engineering environment. This means that chloride contents can be measured independently of these two environmental parameters. However, the sensor is highly sensitive to the alkalinity of the pore solution. Thus, a preliminary expression of the sensor response that considers the interference of alkalinity (OH^- ions) is proposed.

The chloride sensor prototype presented herein offers a cost-effective, easy-to-install and durable sensor system for health monitoring and management of the civil infrastructure subjected to chloride-induced corrosion. The sensors could be deployed in the form of a structural health monitoring system to continuously measure chloride contents in concrete. The information can be used to update the parameters of chloride diffusion models for the prediction of corrosion initiation, maintenance, and service-life performance of concrete structures.

Acknowledgments

The work is supported by the Scientific Research Found of Hunan provincial Education Department of China (22B0473), Royal Society (IEC\NSFC\191350), the National Natural Science Foundation of China, China (No. 52175112).

Figures

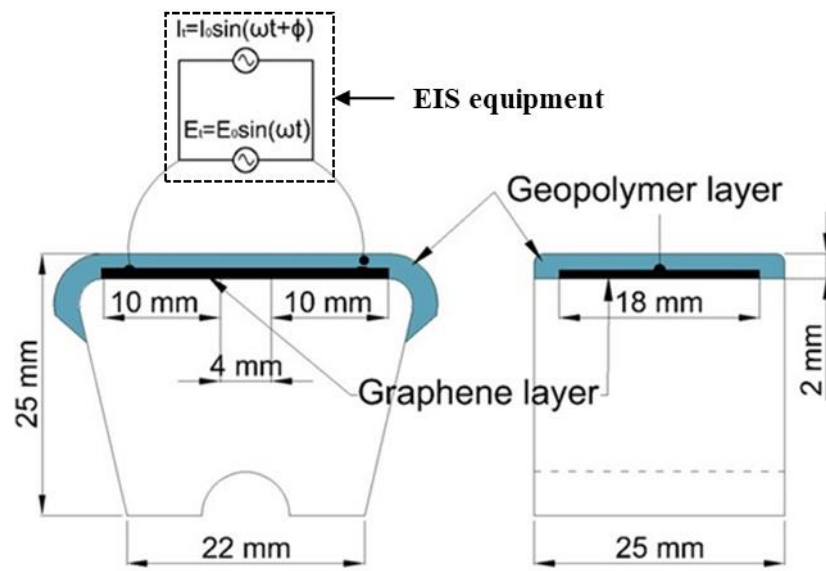


Fig. 1. Layout and size of the chloride sensor.

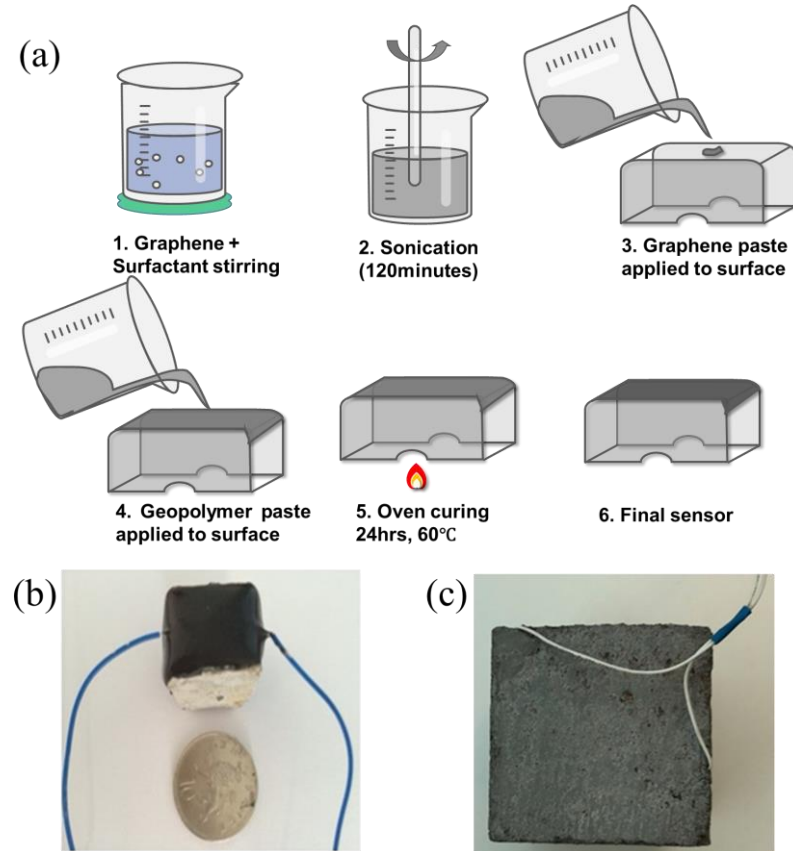


Fig. 2. Chloride sensor (a) manufacturing process, (b) completed chloride sensor, (c) concrete cube with the embedded sensor.

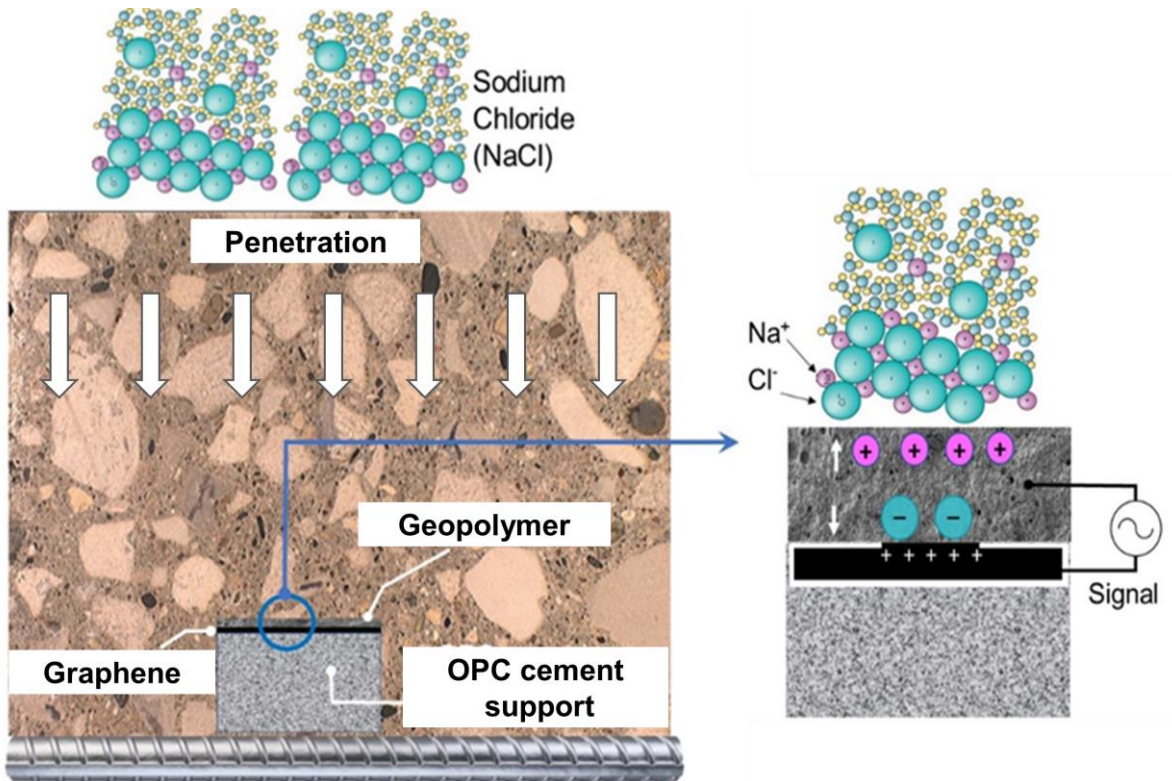


Fig. 3. Chloride sensor working principle.

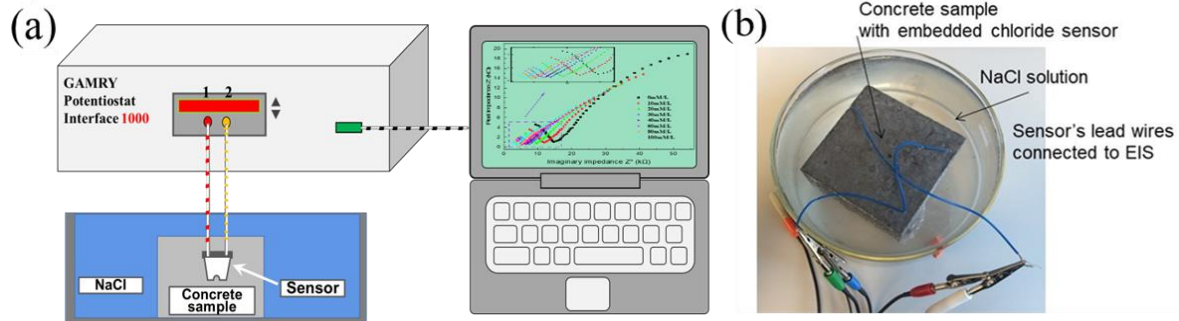


Fig. 4. Experimental test set up for the sensor subjected to NaCl solution.

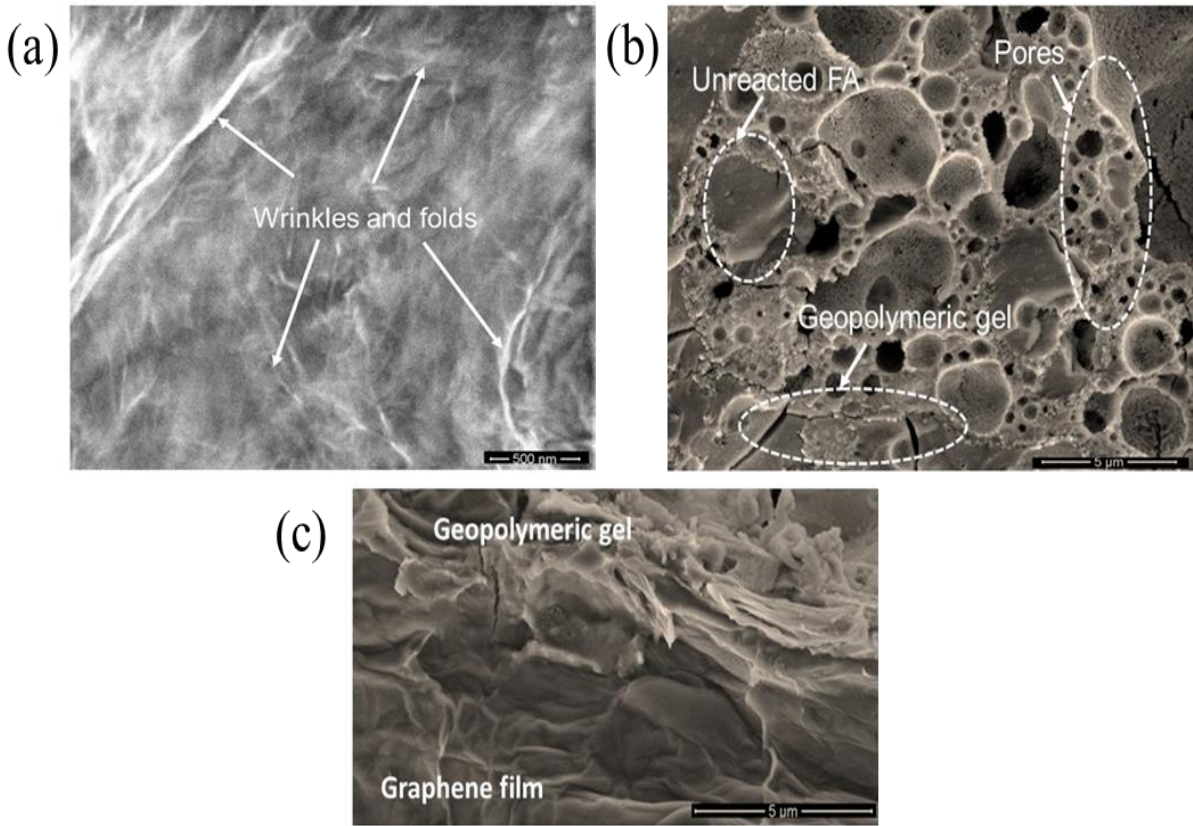


Fig. 5. SEM micro images of (a) Graphene film, (b) Geopolymer microstructure, (c) Geopolymer layer on the graphene film.

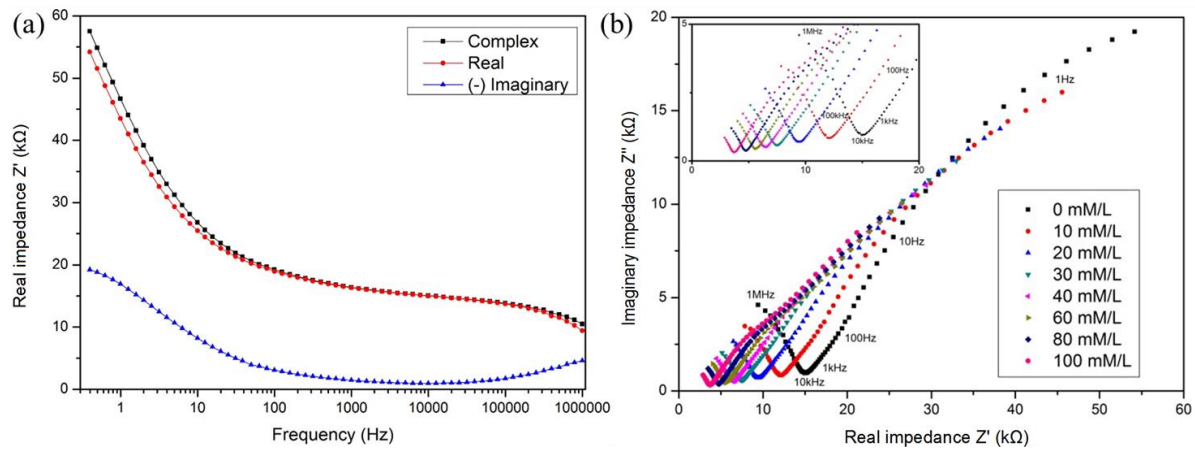


Fig. 6 Impedance of the sensor at room temperature (a) Bode plot prior exposure to chloride, (b) Nyquist plot at different Cl^- concentrations.

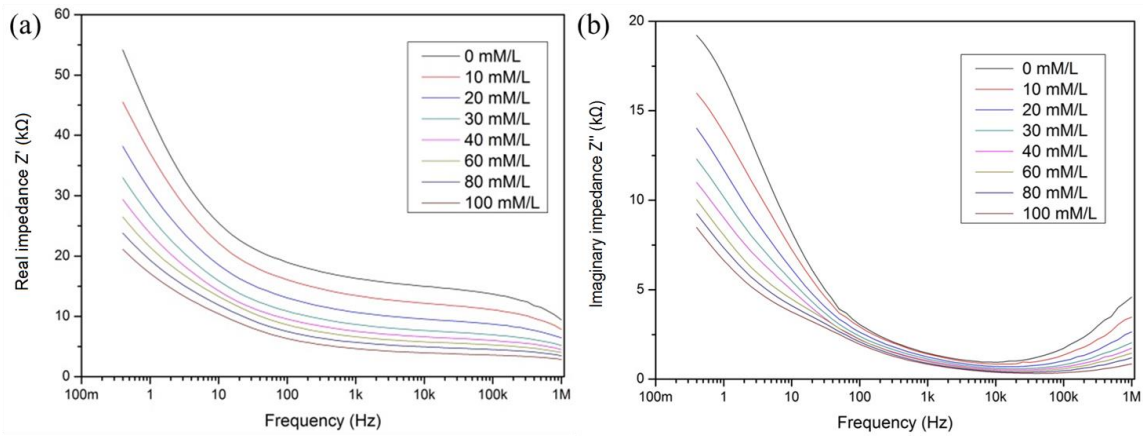


Fig. 7. Bode plot of the sensor at different Cl^- concentrations (a) real impedance, (b) imaginary impedance.

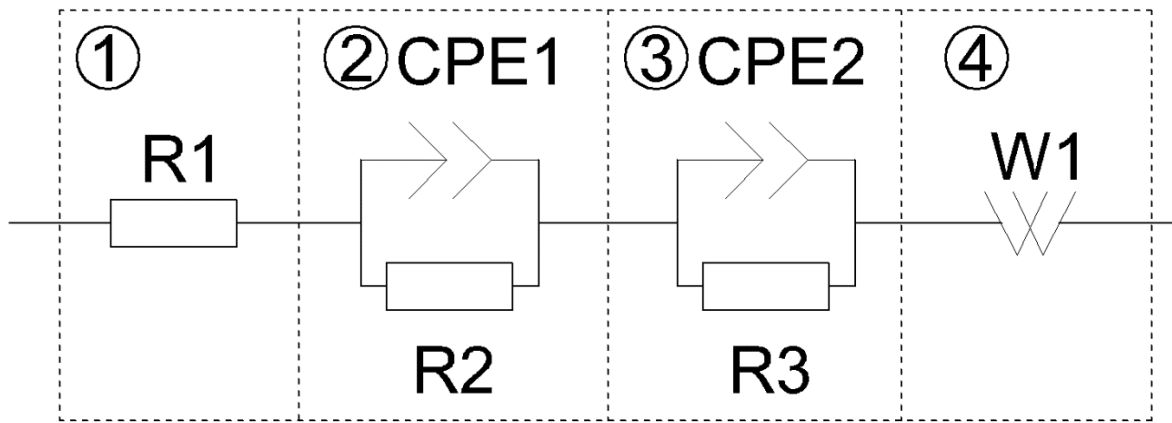


Fig. 8. Equivalent circuit for the sensor.

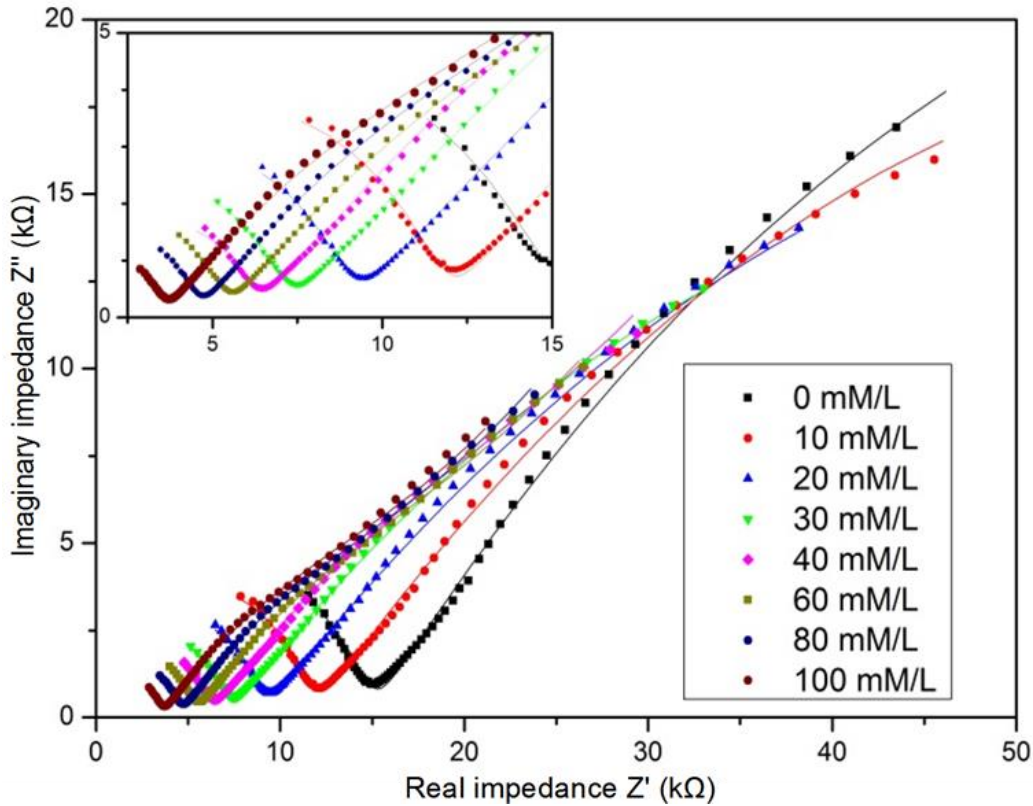


Fig. 9. Nyquist plots for the sensor at different Cl^- concentrations and the corresponding equivalent circuit (solid lines).

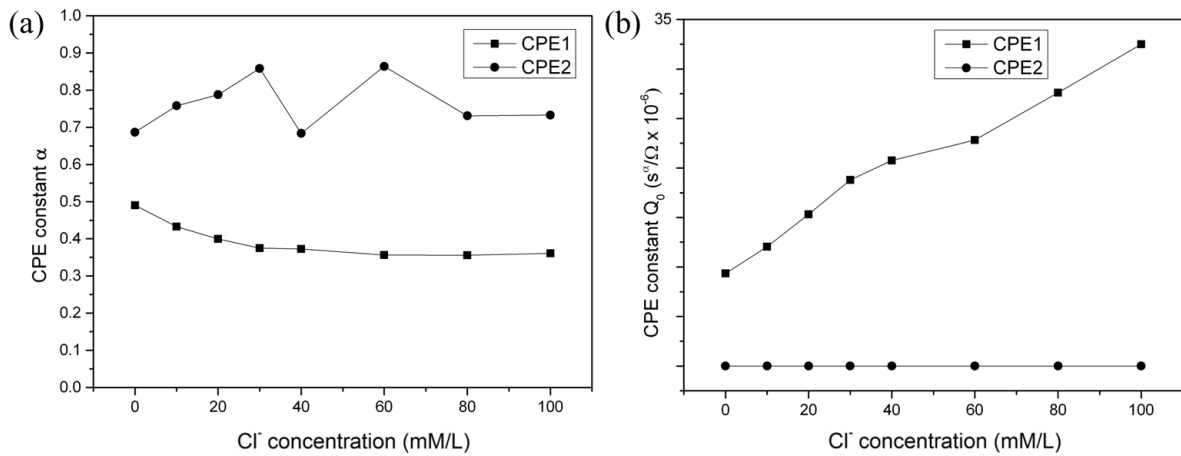


Fig. 10. Effect of Cl^- concentrations on the equivalent circuit parameters for the sensor (a) parameter α and (b) parameter Q_0 .

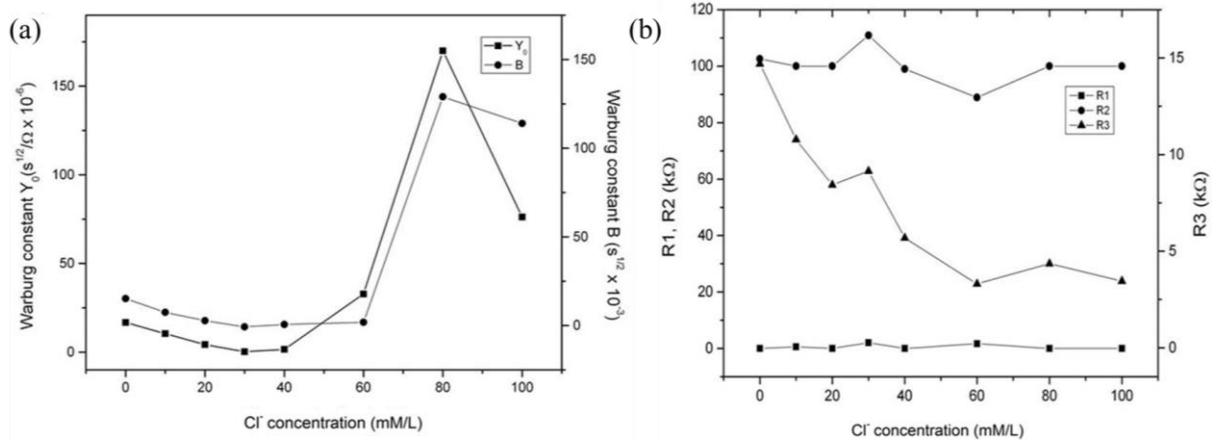


Fig. 11. Effect of Cl^- concentrations on the equivalent circuit parameters for the sensor (a) Warburg elements Y_0 and B , and (b) R_1 , R_2 and R_3 .

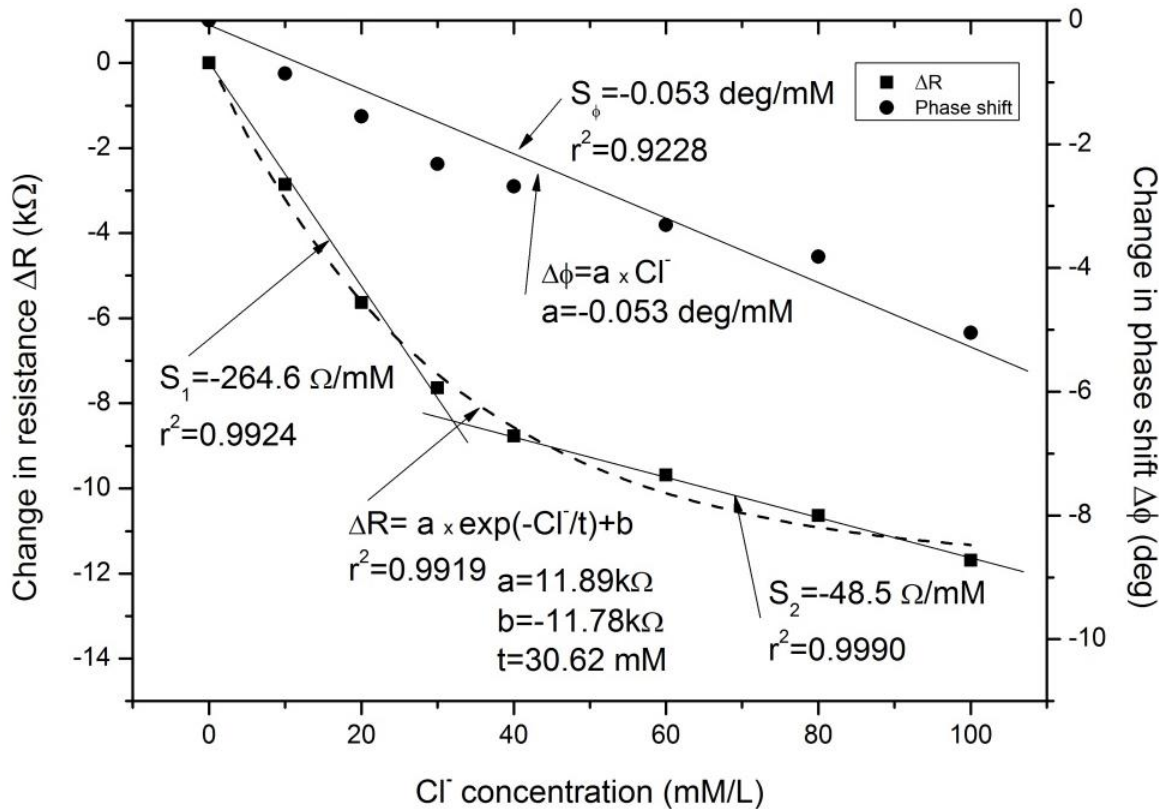


Fig. 12 Sensitivity of the sensor at 1 kHz.

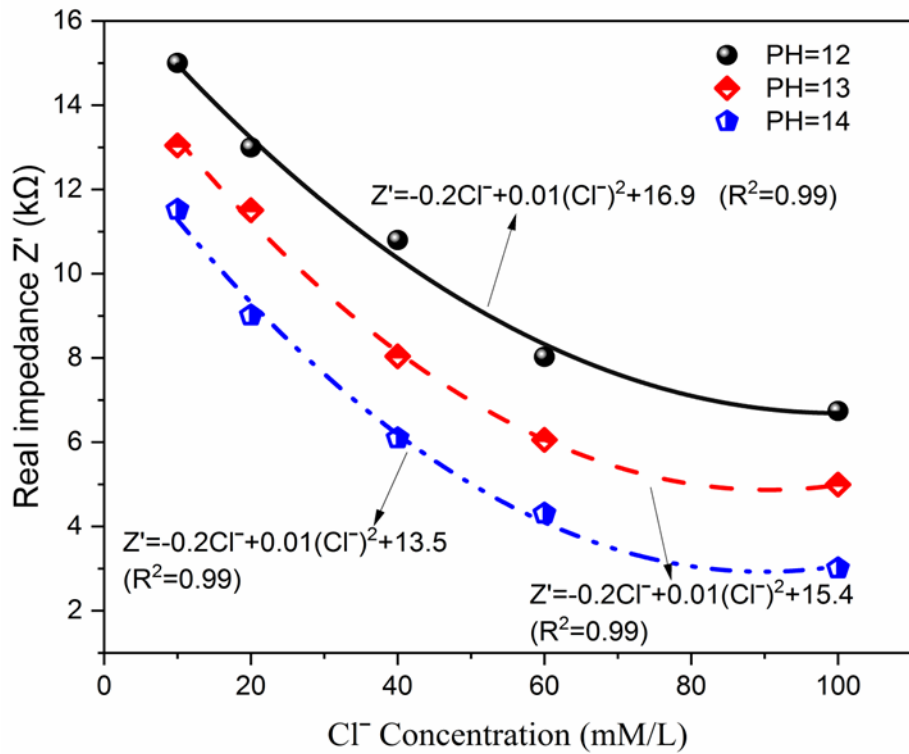


Fig. 13 Effect of pH on the response of the sensor at 1 kHz.

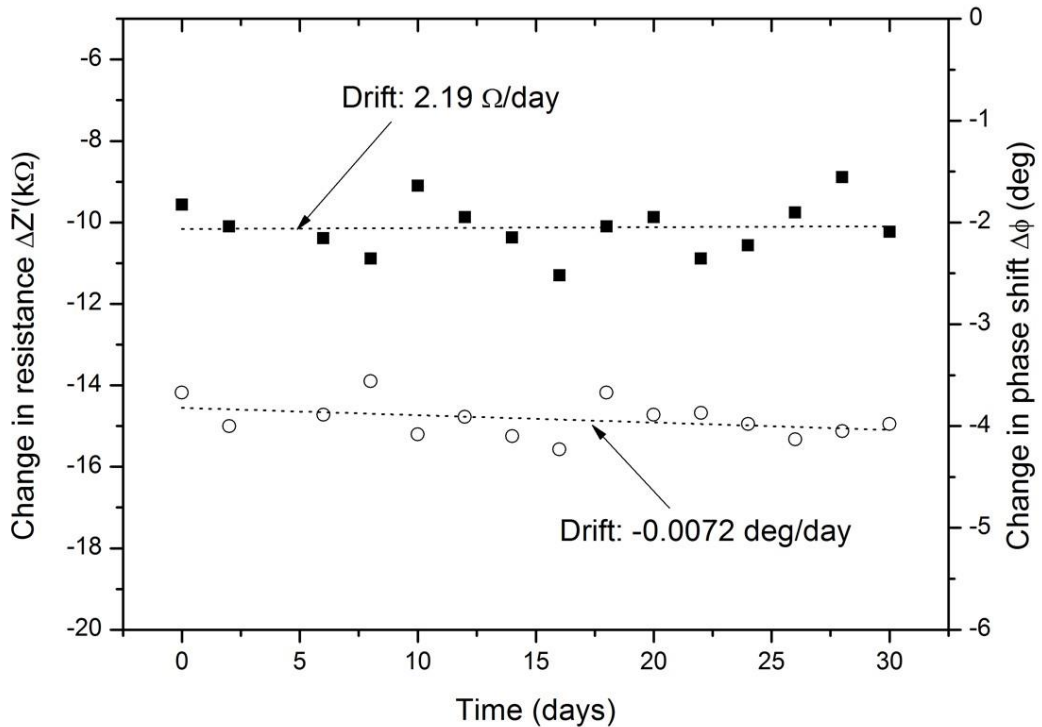


Fig. 14 Stability of the sensor at 1 kHz and 60 mM.

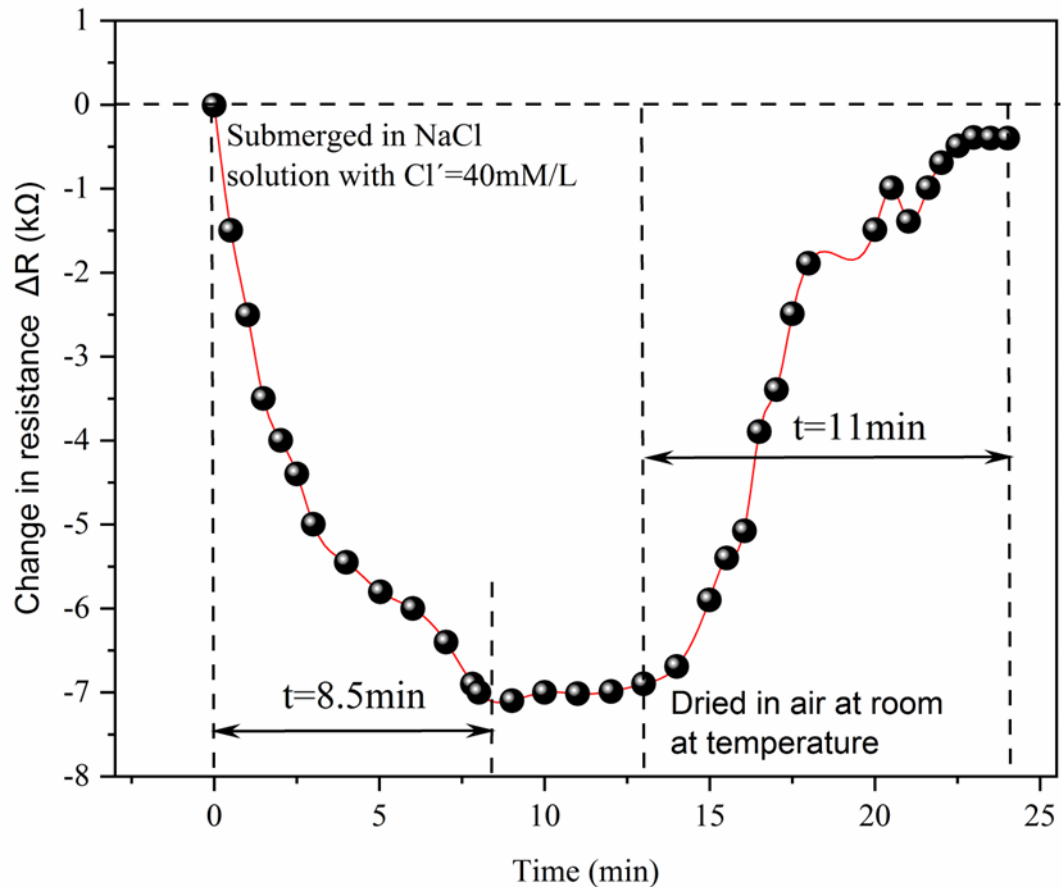


Fig. 15 Reversibility of the sensor under one wet-dry cycle at 1 kHz and 40 mM.

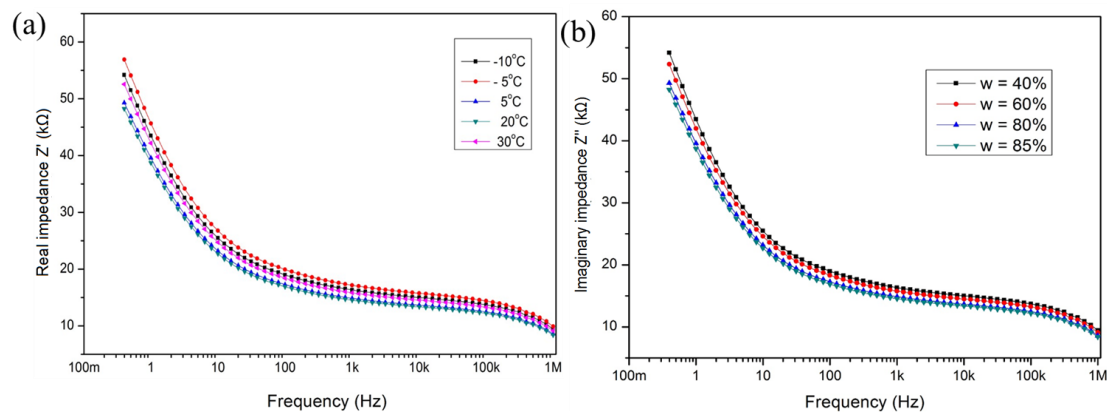


Fig. 16 Sensor at 1 kHz response effect of (a) temperature, (b) humidity.

Reference

- [1] S. Fang, L. Li, Z. Luo, Z. Fang, D. Huang, F. Liu, H. Wang, Z. Xiong, Novel FRP interlocking multi-spiral reinforced-seawater sea-sand concrete square columns with longitudinal hybrid FRP–steel bars: Monotonic and cyclic axial compressive behaviours, *Compos. Struct.* 305 (2023) 116487.
- [2] L. Yu, R. François, V.H. Dang, V. L’Hostis, R. Gagné, Development of chloride-induced corrosion in pre-cracked RC beams under sustained loading: Effect of load-induced cracks, concrete cover, and exposure conditions, *Cem. Concr. Res.* 67 (2015) 246–258. <https://doi.org/10.1016/j.cemconres.2014.10.007>.
- [3] S.P. Karthick, S. Muralidharan, V. Saraswathy, K. Thangavel, Long-term relative performance of embedded sensor and surface mounted electrode for corrosion monitoring of steel in concrete structures, *Sensors Actuators, B Chem.* 192 (2014) 303–309. <https://doi.org/10.1016/j.snb.2013.10.123>.
- [4] G. Zhang, C. Chen, K. Li, F. Xiao, J. Sun, Y. Wang, X. Wang, Multi-objective optimisation design for GFRP tendon reinforced cemented soil, *Constr. Build. Mater.* 320 (2022) 126297. <https://doi.org/10.1016/j.conbuildmat.2021.126297>.
- [5] K.Y. Ann, J.H. Ahn, J.S. Ryou, The importance of chloride content at the concrete surface in assessing the time to corrosion of steel in concrete structures, *Constr. Build. Mater.* 23 (2009) 239–245. <https://doi.org/10.1016/j.conbuildmat.2007.12.014>.
- [6] K.T. Wan, C.K.Y. Leung, L. Chen, A novel optical fiber sensor for steel corrosion in concrete structures, *Sensors.* 8 (2008) 1960–1976. <https://doi.org/10.3390/s8031960>.
- [7] Y.A. Villagrán-Zaccardi, C. Andrade, Chloride ingress rate and threshold content, as determined by the ‘Integral’ test method, in concrete with several w/c ratios in saturated and unsaturated conditions, *Dev. Built Environ.* 8 (2021). <https://doi.org/10.1016/j.dibe.2021.100062>.
- [8] J. Xu, L. Jiang, J. Wang, Influence of detection methods on chloride threshold value for the corrosion of steel reinforcement, *Constr. Build. Mater.* 23 (2009) 1902–1908. <https://doi.org/10.1016/j.conbuildmat.2008.09.011>.
- [9] H. An, G. Meng, Y. Wang, J. Wang, B. Liu, F. Wang, Study on the chloride threshold and risk assessment of rebar corrosion in simulated concrete pore solutions under applied potential, *Coatings.* 10 (2020). <https://doi.org/10.3390/COATINGS10050505>.
- [10] C.L. Page, N.R. Short, W.R. Holden, The influence of different cements on chloride-induced corrosion of reinforcing steel, *Cem. Concr. Res.* 16 (1986) 79–86.

[https://doi.org/10.1016/0008-8846\(86\)90071-2](https://doi.org/10.1016/0008-8846(86)90071-2).

- [11] K. Stanish, M. Thomas, The use of bulk diffusion tests to establish time-dependent concrete chloride diffusion coefficients, *Cem. Concr. Res.* 33 (2003) 55–62.
[https://doi.org/10.1016/S0008-8846\(02\)00925-0](https://doi.org/10.1016/S0008-8846(02)00925-0).
- [12] O.S. and O.E. Gjoryv, Electrical Resistivity Measurements for Quality Control During Concrete Construction, *ACI Mater. J.* 105 (n.d.). <https://doi.org/10.14359/20195>.
- [13] Y. Lecieux, F. Schoefs, S. Bonnet, T. Lecieux, S.P. Lopes, Quantification and uncertainty analysis of a structural monitoring device: Detection of chloride in concrete using DC electrical resistivity measurement, *Nondestruct. Test. Eval.* 30 (2015) 216–232. <https://doi.org/10.1080/10589759.2015.1029476>.
- [14] T.H. Nguyen, T. Venugopala, S. Chen, T. Sun, K.T.V. Grattan, S.E. Taylor, P.A.M. Basheer, A.E. Long, Fluorescence based fibre optic pH sensor for the pH 10-13 range suitable for corrosion monitoring in concrete structures, *Sensors Actuators, B Chem.* 191 (2014) 498–507. <https://doi.org/10.1016/j.snb.2013.09.072>.
- [15] P.L. Fuhr, D.R. Huston, Fiber optic chloride threshold detectors for concrete structures, *J. Struct. Control.* 7 (2000) 77–102.
- [16] G.S. Duffó, S.B. Farina, C.M. Giordano, Characterization of solid embeddable reference electrodes for corrosion monitoring in reinforced concrete structures, *Electrochim. Acta.* 54 (2009) 1010–1020.
<https://doi.org/10.1016/j.electacta.2008.08.025>.
- [17] M.A. Climent-Llorca, E. Viqueira-Pérez, M.M. López-Atalaya, Embeddable Ag/AgCl sensors for in-situ monitoring chloride contents in concrete, *Cem. Concr. Res.* 26 (1996) 1157–1161.
- [18] J.M. Gandía-Romero, R. Bataller, P. Monzón, I. Campos, E. García-Breijo, M. Valcuende, J. Soto, Characterization of embeddable potentiometric thick-film sensors for monitoring chloride penetration in concrete, *Sensors Actuators, B Chem.* 222 (2016) 407–418. <https://doi.org/10.1016/j.snb.2015.07.056>.
- [19] Z. Zhang, J. Hu, Y. Ma, Y. Wang, H. Huang, Z. Zhang, J. Wei, S. Yin, Q. Yu, A state-of-the-art review on Ag/AgCl ion-selective electrode used for non-destructive chloride detection in concrete, *Compos. Part B Eng.* 200 (2020) 108289.
<https://doi.org/10.1016/j.compositesb.2020.108289>.
- [20] T.H.T. Chan, L. Yu, H.Y. Tam, Y.Q. Ni, S.Y. Liu, W.H. Chung, L.K. Cheng, Fiber Bragg grating sensors for structural health monitoring of Tsing Ma bridge: Background and experimental observation, *Eng. Struct.* 28 (2006) 648–659.

<https://doi.org/10.1016/j.engstruct.2005.09.018>.

- [21] C.P. Atkins, M.A. Carter, J.D. Scantlebury, Sources of error in using silver/silver chloride electrodes to monitor chloride activity in concrete, *Cem. Concr. Res.* 31 (2001) 1207–1211. [https://doi.org/10.1016/S0008-8846\(01\)00544-0](https://doi.org/10.1016/S0008-8846(01)00544-0).
- [22] Y. Liu, J. Lynch, The development of chloride ion selective polypyrrole thin film on a layer-by-layer carbon nanotube working electrode, in: Proc.SPIE, 2011.
<https://doi.org/10.1117/12.880063>.
- [23] M. Jin, L. Jiang, M. Lu, S. Bai, Monitoring chloride ion penetration in concrete structure based on the conductivity of graphene/cement composite, *Constr. Build. Mater.* 136 (2017) 394–404. <https://doi.org/10.1016/j.conbuildmat.2017.01.054>.
- [24] H.K. Kim, Chloride penetration monitoring in reinforced concrete structure using carbon nanotube/cement composite, *Constr. Build. Mater.* 96 (2015) 29–36.
<https://doi.org/10.1016/j.conbuildmat.2015.07.190>.
- [25] L. Biondi, M. Perry, J. McAlorum, C. Vlachakis, A. Hamilton, G. Lo, Alkali-Activated Cement Sensors for Sodium Chloride Monitoring, *IEEE Sens. J.* 21 (2021) 21197–21204. <https://doi.org/10.1109/JSEN.2021.3100582>.
- [26] L. Biondi, M. Perry, J. McAlorum, C. Vlachakis, A. Hamilton, Geopolymer-based moisture sensors for reinforced concrete health monitoring, *Sensors Actuators, B Chem.* 309 (2020) 127775. <https://doi.org/10.1016/j.snb.2020.127775>.
- [27] A. Benhamouda, J. Castro-Gomes, Preliminary Study of the Rheological and Mechanical Properties of Alkali-activated Concrete Based on Tungsten Mining Waste Mud, *KnE Eng.* 2020 (2020) 101–110. <https://doi.org/10.18502/keg.v5i4.6801>.
- [28] A. Revil, D. Jougnot, Diffusion of ions in unsaturated porous materials, *J. Colloid Interface Sci.* 319 (2008) 226–235. <https://doi.org/10.1016/j.jcis.2007.10.041>.
- [29] S. Karthick, S.J. Kwon, H.S. Lee, S. Muralidharan, V. Saraswathy, R. Natarajan, Fabrication and evaluation of a highly durable and reliable chloride monitoring sensor for civil infrastructure, *RSC Adv.* 7 (2017) 31252–31263.
<https://doi.org/10.1039/c7ra05532c>.
- [30] M. Jin, L. Jiang, D. Tao, S. Bai, Characterization of Ag/AgCl electrode manufactured by immersion in sodium hypochlorite acid for monitoring chloride content in concrete, *Constr. Build. Mater.* 122 (2016) 310–319.
<https://doi.org/10.1016/j.conbuildmat.2016.05.163>.
- [31] G. De Vera, M.A. Climent, C. Antón, A. Hidalgo, C. Andrade, Determination of the selectivity coefficient of a chloride ion selective electrode in alkaline media simulating

- the cement paste pore solution, *J. Electroanal. Chem.* 639 (2010) 43–49.
- [32] Y.S. Femenias, U. Angst, F. Caruso, B. Elsener, Ag/AgCl ion-selective electrodes in neutral and alkaline environments containing interfering ions, *Mater. Struct.* 49 (2016) 2637–2651.
- [33] Z. Abdollahnejad, F. Pacheco-Torgal, T. Félix, W. Tahri, J. Barroso Aguiar, Mix design, properties and cost analysis of fly ash-based geopolymers foam, *Constr. Build. Mater.* 80 (2015) 18–30. <https://doi.org/10.1016/j.conbuildmat.2015.01.063>.
- [34] M. Tian, Y. Huang, W. Wang, R. Li, P. Liu, C. Liu, Y. Zhang, Temperature-dependent electrical properties of graphene nanoplatelets film dropped on flexible substrates, *J. Mater. Res.* 29 (2014) 1288–1294. <https://doi.org/10.1557/jmr.2014.109>.

Declaration of interests

The authors declare that they have no known competing financial interests or personal relationships that could have appeared to influence the work reported in this paper.

The authors declare the following financial interests/personal relationships which may be considered as potential competing interests:

Bo Huang is the Deputy Director of Bridge Structure and Materials Institute and an Associate professor in the Engineering College at Hunan university of science and technology, China. He obtained his MSc degree in project management from Manchester University, UK, in 2015. He received his PhD degree in Engineering at Lancaster University in 2021. His research interests lie in a broad range of civil engineering areas, including fibre-reinforced composites, material characterisation and bio low-carbon engineered cementitious composites.

Jianqun Wang received the BE, ME, and Dr. Eng. degrees in bridge and tunnel engineering from Hunan University, Changsha, China, in 2005, 2007, and 2011, respectively. In 2011, he joined Hunan University of Science and Technology as a lecturer. Subsequently, he was promoted to associate professor of Hunan University of Science and Technology in 2017. From 2019 to 2020, he was a visiting scholar at the University of Houston, Houston, U.S.A. He was promoted to professor of Hunan University of Science and Technology in 2022.

Gabor Piukovics gained his bachelor's degree in engineering on 2013, with thesis focused on the Hybrid graphene/geopolymeric cement as a superionic conductor for structural health monitoring applications.

Niloufar Zabihi gained her PhD degree in Engineering on 2022 at Lancaster University, with the thesis Converting Road Kinetic Energy to Electricity for Smart City Infrastructure.

Ye Junjie, Professor, doctoral supervisor. In 2011, he graduated from Xi'an Jiaotong University, majoring in mechanical manufacturing and automation. In 2012, he entered Xidian University, mainly engaged in finite element theory and mechanical system damage modeling method research. In recent years, more than 30 SCI papers have been published. The research interest is multi-field coupling theory of intelligent structures. The rapid development of modern aerospace requires equipment with high safety and high reliability. The harsh service environment is proposed to improve the use of intelligent composite material structures. more severe test.

Mohamed Saafi is a Professor and Chair at Lancaster University. Prof. Saafi's research group works in cutting-edge and multidisciplinary areas of materials science, computing, energy harvesting and storage, artificial intelligence (AI) and structural health monitoring in the context of sustainable, resilient and smart Built Environment. Prof Saafi's research areas in materials science include the design of novel low-carbon cementitious and polymer composite materials using nanomaterials, design of carbon-negative infrastructure materials using CO₂ and waste, upcycling of plastic waste towards the design of structural materials, and multifunctional sea-water, sea-sand and sea-aggregate concrete materials.

Jianqiao Ye is a Professor and the Chair of Mechanical Engineering at Lancaster

University and a member of the Lancaster Intelligent, Robotic and Autonomous Systems Centre (LIRA). Jianqiao's research covers a broad range of both academic and industrial interests, including failure and damage of fibre reinforced composites, advanced steel-concrete composite structures, geopolymers, lighter and green cementitious materials, cement and concrete carbonation, offshore oil and gas structures and vibration energy harvesting. He has worked on testing, numerical modelling and optimization of a wide range of materials and structures, which has been extended to the applications of modern analytical instruments such as X-CT, SEM, XRD, EDS, and data-driven techniques, including metamodeling, machine learning and digital twins.

Author's contribution

Bo Huang, Gabor Piukovics, Niloufar Zabihi, Junjie Ye, Mohamed Saafi, Jianqiao Ye: conceptualization; methodology.

Bo Huang, Gabor Piukovics, Niloufar Zabihi, Junjie Ye: data curation; formal analysis; visualization.

Mohamed Saafi, Jianqiao Ye, Junjie Ye: funding acquisition; supervision; resources.

Bo Huang, Gabor Piukovics, Niloufar Zabihi, Junjie Ye: investigation; validation; roles/writing – original draft.

Mohamed Saafi: project administration.

Mohamed Saafi, Jianqiao Ye: writing – review & editing.